Title

STRENGTHENING EFFECTS OF SPINODAL DECOMPOSITION IN GOLD-PLATINUM ALLOYS AND THE KINETICS OF THE REACTION

Author

Carpenter, Ray Warren.

Publication Date

1966

UCRL-16609

University of California

Ernest O. Lawrence Radiation Laboratory

STRENGTHENING EFFECTS OF SPINODAL DECOMPOSITION IN GOLD-PLATINUM ALLOYS AND THE KINETICS OF THE REACTION

Berkeley, California

DISCLAIMER

UCRL-16609

UNIVERSITY OF CALIFORNIA

Lawrence Radiation Laboratory
Berkeley, California

AEC Contract W-7405-eng-48

STRENGTHENING EFFECTS OF SPINODAL DECOMPOSITION IN GOLD-PLATINUM ALLOYS AND THE KINETICS OF THE REACTION

Ray Warren Carpenter

(Ph.D. Thesis)

January 1966

TABLE OF CONTENTS

STRENGTHENING EFFECTS OF SPINODAL DECOMPOSITION IN GOLD-PLATINUM ALLOYS AND THE KINETICS OF THE REACTION

Ray Warren Carpenter

Inorganic Materials Research Division, Lawrence Radiation Laboratory,
Department of Mineral Technology, College of Engineering,
University of California, Berkeley, California

ABSTRACT

January 1966

Stress-strain characteristics, fracture, and reaction kinetics of two gold-platinum alloys in various stages of spinodal decomposition have been experimentally investigated. The size of the structural modulations produced by spinodal decomposition ranged from about 20 to 40 lattice constants and the reaction rate time dependence followed a law similar to those derived to represent the coalescence of spheres. The temperature dependence of the reaction rate agreed well with that of chemical diffusion in this alloy system. It was found that spinodally hardened alloys had a very high work-hardening rate, the yield strength increased upon decomposition, and the alloys were embrittled by this reaction, fracture occurring through the grain boundaries. A theory was proposed to explain the high work-hardening rate, and the brittle grain boundary fracture was attributed to precipitation at the grain-boundaries of soft, incoherent grains of the equilibrium phases.

A. INTRODUCTION

The principal objectives of this investigation were the experimental determination of the effects of spinodal decomposition on the mechanical properties of certain alloys, and the temperature dependence of the reaction rate. The decomposition of a solid solution by the process called "spinodal" is a special form of solid state precipitation reaction. Since the concept is not well known, a brief description will be given herein.

The term "spinodal" is of thermodynamic origin, and for a binary alloy denotes the points X_i (i=1,2) at which $\frac{\partial^2 F}{\partial X_i^2} = 0$ on a (Gibbs) free energy-composition diagram for fixed temperature. This is schematically illustrated in Fig. 1 for the gold-platinum system. The solid curve shown in the bottom portion of the figure represents the free-energy of the metastable supersaturated solid solution as a function of composition at the temperature T_1. The boundaries of the two phase field ($\alpha_1 + \alpha_2$) at T_1 on the phase diagram are given by the intersections of the common tangent with the matastable solution free energy curve. The spinodal points at T_1 are given by the inflexion points of the free-energy curve and are marked by the innermost pair of vertical dotted lines from the free-energy curve up to the T_1 line on the phase diagram. The dotted lines within the $\alpha_1 + \alpha_2$ field boundaries on the phase diagram mark the locus of spinodal points for all temperatures where the $\alpha_1 + \alpha_2$ phase field exists.

The significance of the spinodal curve for precipitation reactions can be seen by considering $\alpha \rightarrow \alpha_1 + \alpha_2$ precipitation reactions for alloys with average compositions inside and outside the spinodal region of the diagram. For example, consider an α alloy of average composition A,

cooled to T_1 where the α solution is unstable. It is usually assumed that a precipitation reaction begins with local composition fluctuations within the α solution; when such a fluctuation occurs in the alloy A the composition of the now segregated metastable solution is represented by a chord on the metastable free-energy curve connecting the composition points of the fluctuation. The figure shows the chord lies below the curve; this is a consequence of the downward concavity between the spinodal points. Thus any small fluctuation for an alloy of average composition between the spinodal points will cause a decrease of the metastable solution free energy and is stable. On the other hand, the same type fluctuation in an alloy of average composition B, where B is between either of the spinodal points and the two phase field boundary, will cause an increase in free energy because the free energy curve is concave upward in these regions; then the fluctuation is unstable and will tend to disappear (see B on free energy diagram of Fig. 1). The concept of spinodal decomposition is clearly that of homogeneous nucleation (i.e., no thermal activation is required) of precipitate in the solid state, within the spinodal region of the two phase field. This concept was apparently first applied to solid state precipitation by Borelius.[1,2]

The approach taken by Borelius is elegant for its simplicity and clarity but it is strictly qualitative and gives no information on the type of structure to be expected. More recently, Hillert[3] and Cahn[4,5] have developed thermodynamic treatments of the transformation that allow structural predictions. Hillert approached the problem by considering changes in solution free energy accompanying composition fluctuations in a single crystallographic direction in the unstable solid solution (i.e., at a temperature within the $\alpha_1 + \alpha_2$ phase field), also accounting for the

effect of surface energy resulting from the composition fluctions. He was able to show analytically that the activation energy barrier for nucleation was very low throughout the two phase regions and disappeared completely in the vicinity of the spinodal lines; surface energy prevents the decomposition from occurring on too fine a scale. Using the derivative with respect to position in the lattice of his free energy expression, Hillert defined a diffusion equation for the growth of the structure resulting from spinodal decomposition. The solutions to this equation for small composition fluctuations are periodic, leading to a wave-like distribution of fine coherent precipitate nuclei throughout the volume of solution. Cahn's theoretical treatment uses basically the same approach, however, he included a term in the free energy equation to account for the elastic strain energy due to coherency of the "nuclei" with the initial matrix and restricted the treatment to infinitesimal composition fluctuations. This restriction allowed the extension of the treatment to three dimensional composition fluctions. This treatment also gives a periodic distribution of the growth centers of the equilibrium phases. The inclusion of strain energy modifies the spinodal curve, requiring a greater thermodynamic driving force to cause the spinodal reaction in the presence of strain energy, but does not change the predicted precipitate morphology. Both Cahn and Hillert's theory are mathematically complex. They will not be dealt with in detail here, but the results will be used when convenient.

The crystallographic changes occurring during spinodal decomposition have been investigated by x-ray diffraction in the gold-platinum system by Tiedema, et al.[6] and Van der Toorn[7] and in the Fe-Cu-Ni system by Daniel and Lipson,[8] Hargreaves,[9] and Hillert. et al.[10] An unusual x-ray diffraction effect termed "sidebands" was observed on Debye-Scherrer photographs

accompanying changes in the stress-strain behavior of the alloys were correlated with λ. The Au-Pt system was chosen because it has the largest difference in constituent atom sizes of any known spinodal system[12] and thus the changes in mechanical properties should be large.

B. EXPERIMENTAL METHODS

1. Alloy Specimen Preparation

All specimens used for tensile and diffraction experiments were in the form of 0.020 inch diameter wires. The wires were made* from ingots which were induction melted in zirconium silicate crucibles. The atmosphere during all melting and fabrication was air. After melting the alloys were cast directly into graphite molds for solidification and then water quenched as quickly as possible. Ingot size was 5/8-inch diameter and 5 inches long. Prior to fabrication the alloys were annealed at 900°C and then cold swaged to 1/10-inch in diameter. The wires were cold drawn to final diameter, with appropriate intermediate annealing.

Spectrographic analysis for metallic impurities (semi-quantitative) done by two different laboratories** showed the major contaminants to be Rh (< .04%), Pd (< .07%), Fe (< .04%); all others less than 0.01%. Particular attention was given to silicon concentration. One investigator gave the silicon concentration as 0.0005%, the other was unable to detect silicon.

Gravimetric chemical analysis was carried out on the alloys to determine gold concentration, platinum being obtained by difference. The

---

*Alloy melting and fabrication into wires was done by Englehard Industries, Inc., New Jersey.

**American Spectrographic Laboratories, San Francisco and Englehard Industries, Inc.

results were 20.00 ± 0.01 wt-% Au in the 20-80 alloy and 60.585 ± .005 wt-% in the 60-40 alloy.

2. Specimen Heat Treatment

Tensile specimens were homogenized by resistance heating using a direct current power supply. The experimental arrangement is shown in Fig. 2. The homogenization treatment was terminated by quenching with room temperature helium gas. The copper quench tubes shown in the figure were connected to two solenoid operated vacuum type gate valves on a helium reservoir tank maintained at about 13 psig. The inlet solenoid valve was opened at the same time the heating current was turned off and after a present time the outlet valve opened to prevent too large a pressure rise in the bell jar. With both valves open the steady state helium pressure was about 7 psig. All homogenization treatments were conducted at a pressure of 1 atm in argon. Temperature was measured during homogenization using a Leeds and Northrup disappearing filament optical pyrometer. Since spectral emittance of a metal is dependent upon the condition of the heated surface as well as the metal itself this correction factor was measured directly. A platinum/platinum-10% rhodium thermocouple was spot welded directly on the specimen at approximately the center point of the 3.25 inch length. The thermocouple wires were 0.002 inch diameter to minimize error due to conduction loss down the thermocouple wires. The specimen was then heated to a steady, predetermined temperature and the temperature was measured simultaneously with the thermocouple and optical pyrometer. This was done for both the 60-40 and 20-80 specimens over the true temperature range 921 to 1048° C. The emittance value found was 0.37 ± 0.02 at a wavelength of 6500Å. The uncertainty in the temperature measurement with the optical

pyrometer, which was calibrated by the Radiation Laboratory instrument shop, is ± 5°C. This emittance value is a system parameter because it was measured through the pyrex bell jar; no calibrations were made for glass absorption of the emitted radiation.

Temperature gradients along the sample length were measured using a traversing device for the optical pyrometer. With the center point of the specimen at 1220°C, the temperatures 1 inch above and 1 inch below were within 8°C of 1220°C, which is within 1%. The gage length of the tensile specimens is the central 1 inch; the temperature distribution over this section was isothermal, within the experimental uncertainty.

Isothermal aging heat treatments were carried out by immersing the specimen in a molten salt bath (a mixture of sodium nitrite and sodium nitrate) for the required time-temperature cycles. Salt bath temperature was measured by a chromel-alumel thermocouple connected to a portable potentiometer of ± 0.01 millivolt sensitivity (0.25°C). All furnace control and temperature monitoring thermocouples were checked for proper voltage output at 100°C against a mercury in glass thermometer. Maximum difference noted was less than 2°C. The salt bath was contained in an open top cylindrical pot about 10 inches deep and 2.5 inches in diameter; the temperature gradient within the salt from 1/2-inch below the surface to a depth of 4.5 inches was found to be about 3°C using a thermocouple probe and the bath temperature oscillated ± 2°C around the set point temperature during the aging experiments. The aging temperatures are considered to be accurate within ± 3°C of the specified value, except for times longer than 12 hrs. For long aging treatments the uncertainty is ± 10°C because of furnace drift overnight.

3. Tensile Tests

Because of the limited ductility found in aged specimens it was necessary to devise a gripping technique that would not deform the wires at the points of contact. The grips developed are shown disassembled, with the alignment jig in Fig. 3. The small diameter stainless steel grip tubes were 0.093 in O.D.× 0.023 in I.D.× 1.25 inches long with steel snap rings fitted to the outer ends. The brass grips were drilled and broached to provide a slip fit with the tube. The tensile specimens, 3.25 inches in total length, were fastened inside the stainless steel grip tubes using an epoxy resin; the gripped length was approximately 7/8 inch on each end. The free span between brass grips was 1.5 inches. The assembled tensile specimen and grip assembly was placed in the aluminum alignment jig, as shown in Fig. 3, before the resin was cured. With the alignment jig fastened shut, so that the whole specimen-grip assembly was a rigid unit, the resin was cured at 60°C. The alignment jig was not removed until the specimen was in the tensile machine, with a slight preload applied.

Tensile tests were made in an Instron constant strain-rate testing machine. All tests were run at a constant strain rate of 0.005 inches per minute. The elongation was measured directly, using the central inch of the free span of the specimen as a gage length, by attachment of an electrical extensometer (Instron model No. G-51-11 , sensitivity 5×10^{-5} inch) directly on the wire. The experimental results were displayed directly as a load-strain curve on an X-Y recorder. A special alignment device (Riehle No. 86781) was used in the load train directly above the upper specimen grip to minimize the effect of any bending moments in the grip specimen assembly. This device functioned as a set of crossed knife

edges with lever arms extending out 7 inches from the load train axis at 90° intervals. Bending moments were measured by linear differential transformers at the ends of the lever arms and a null-balance circuit and removed from the load train by adjusting the knife edges until the transducers indicated zero net moment.

4. X-Ray Diffraction Measurements

All diffraction pictures were taken with 114.6 cm diameter Debye-Scherrer cameras; nickel filtered copper radiation was used. The 0.020 inch diameter aged tensile specimens were photographed in a camera suitably modified to accept specimens of this length. Sideband measurements for study of reaction kinetics were made on shorter lengths of wire.

Lattice constants determined for the alloys in the homogenized and quenched condition are:

Alloy (Au-Pt)	a_0, Å	Number of specimens examined
60-40	4.015 ± .001	5
20-80	3.954 ± .001	4

The lattice constants reported for these alloys by Darling, et al. are 4.012 ± .001Å and 3.958 ± .003Å for the 60-40 and 20-80 alloys, respectively. Each of these values is the result of two determinations. To investigate this discrepancy the surface of several wires of each composition was etched and rephotographed several times. It was found that the lattice constant of the 60-40 alloy was about 4.013Å in the unetched condition; it increased to 4.015 ± .001 after the first etch and remained at this value thereafter, indicating surface gold depletion during homogenization (the lattice constant of pure gold is larger than that of pure platinum). The etching treatments on the 20-80 alloys did not show this effect, within the

experimental limits. Since the effect was found in one of the alloys, all specimens were etched before diffraction examination. In addition, several specimens subjected to repeated aging in the molten salt bath were etched and rephotographed between aging treatments to determine whether the salt was responsible for any effects attributed to spinodal reaction. No changes caused by reaction with the salt were found. This is considered sufficient evidence that the reaction is not confined to the specimen's surface.

5. Metallographic Technique

Specimens were mounted in an epoxy resin that would satisfactorily cure at 60°C. The resistance of a quenched 60-40 specimen was monitored for 24 hours at 60°C and no change was observed. It was concluded that significant room temperature aging does not occur in these alloys. Polishing was done in the usual way, using chromic oxide, or aluminum oxide, as the final polishing abrasive. The specimens were electrolytically etched in an aqueous solution consisting of 90% distilled water and 10% saturated KCN(aq) solution. The current density and time were variable depending on whether the primary interest was grain boundary detail or the grains themselves.

6. Microhardness Measurements

Hardness of grains and grain boundary regions of wires mounted with the cylindrical axes horizontal and polished (and etched) to give a flat plane of width slightly less than the wire diameter were measured with a Leitz Miniload Hardness Tester. A 25 gram load and Vickers pyramid indenter were used for all measurements.

C. EXPERIMENTAL RESULTS

1. X-Ray Diffraction Measurements of the Structure During Spinodal Decomposition

The structure of alloys containing 60% Au-40% Pt and 20% Au-80% Pt as a function of isothermal annealing time was calculated from measurements of sideband spacing on Debye-Scherrer photographs using the Daniel-Lipson relation given above (Eq. (1)). Investigations were made for the two alloys at three temperatures: 602, 552, and 502 °C. Figures 4a, b and Figs. 5a, b show Debye-Scherrer films of the 20-80 and 60-40 compositions aged for increasing times at 602°C., respectively (films for aging experiments at other temperatures are compiled in Appendix B). Neither alloy in the homogenized and quenched state shows evidence of diffuse scattering. Weak, diffuse sidebands first appeared after one minute aging treatment and gain intensity and definition with aging time. The angular displacement between sidebands and the parent Bragg reflection decreases with increasing time, indicating an apparent wavelength growth. All measurements of sideband spacing relative to the parent Bragg lines were made on the (200) and (220) lines. This minimizes the uncertainty in sideband position resulting from resolution of the K_α doublet at higher angles. The average wavelengths calculated are given in tabular form in Tables I and II and shown in Figs. 6 and 7. It can be seen that in all cases where short annealing times were investigated the slope of the curve decreases to a lower value than the central portion of the curve, which is linear, and at long annealing times the slope begins to increase. Referring to Figs. 4a, b and Figs. 5a, b, the relatively flat portion of the curve occurs when the sideband intensity is weak and most diffuse,

Table I. Average Wavelength vs Aging Time for 20 Au-80 Pt Alloys
(Wavelength in Lattice Constants)

Agetime (min)	λ_{200}	λ_{220}	Comments
30			Sidebands present but not measureable
120	16 ± 3	19 ± 3	
300	18	20	
600	22	24	
900	30	25	
1200	35	32	Low angle sideband replaced by streaks.
	Aged at 552°C		
10	15	14.0	
30	17	15	
60	20	21	
180	28	27	Low angle sideband intensity low
300	35	36	Low angle sideband replaced by streaks
	Aged at 602°C		
1	15.6		sidebands very diffuse
3	16	17	
9	19	19	
12	20	22	
15	23	24	
18	24	24	
21	24	25	
24	26	26	
27	27	26	
60	35	38	
90	48	42	Low angle sideband replaced by streak

Table II. Average Wavelength vs Aging Time for 60 Au-40Pt Alloys
(Wavelength in Lattice Constants)

Agetime (min)	λ_{200}	λ_{220}	Comments
120	18	--	
300	23	21	
480	24	23	
600	26	24	
905	30	26	
1200	34	28	
		Aged at 550°C	
10	17	15	
30	20	19	
60	23	22	
180	30	27	
300	34	30	
		Aged at 602°C	
1	--	--	Sidebands present; too undefined to measure.
3	21	20	
9	23	22	
12	24	23	
15	25	22	
18	28	23	
21	26	26	
24	26	27	
27	27	27	
60	32	35	
90	40	35	High angle sideband replaced by streaks.

and the linear portion to an intermediate stage where sideband intensity is greater and the bands are more well defined. The measurements of sideband position for the calculation of wavelengths were made at the intensity maximum within the sideband. In the later stages of reaction the low angle sideband for 20-80 alloys and high angle sideband for 60-40 alloys have been replaced by streaks, but the conjugate sideband is still present in each case. This stage of the reaction corresponds to the increase in slope of the growth curves, Figs. 20 and 21. The two sidebands of a pair also show an asymmetric intensity distribution. The linear section of each curve has been assumed to represent a steady-state reaction rate in each case, and an equation to fit this section of each curve has been calculated by the method of least squares and are tabulated in Table III.

Table III. Equations for Steady State Spinodal Reaction Rate in Gold-Platinum Alloys.

Aging Temperature	Equation
60% Au-40% Pt	
502°C	$\log \lambda = 0.21 \log t + 0.81$
552°C	$\log \lambda = 0.20 \log t + 1.00$
602°C	$\log \lambda = 0.22 \log t + 1.13$
20% Au-80% Pt	
502°C	$\log \lambda = 0.32 \log t + 0.47$
552°C	$\log \lambda = 0.30 \log t + 0.77$
602°C	$\log \lambda = 0.32 \log t + 0.98$

Units: λ in lattice constants
t in minutes

2. Mechanical Properties

The stress-strain characteristics of alloys containing 60% Au-40% Pt quenched and aged at 510°C are shown in Fig. 8. Mechanical property measurements for other specimens aged at 510°C for successively longer times are given in Table IV. The stress-strain curves for these tests are included in Appendix A.

The most pronounced change accompanying aging was the large increase in work hardening rate and the abrupt decrease in plastic strain evident from the beginning of the precipitation reaction. The initial yield point increases by about 25% during the first one-half hour of aging and approaches a constant value about 50% higher than the homogeneous quenched alloy after 5 hours at 510°C. Another group of specimens was aged at 410°C to investigate mechanical property changes at earlier stages of the reaction. The results obtained are given in Table V and characteristic stress-strain curves for various stages of the reaction are shown in Fig. 9. (All stress-strain curves for this aging temperature are included in Appendix A.) The work hardening rates for these curves at small plastic strain, show a gradual increase with aging time and the other general characteristics are the same as those observed at 510°C. The work hardening rate, which is defined as the slope of the stress-strain curve, was calculated graphically for all stress-strain curves at a plastic strain of 2.5×10^{-3}. The selection of this value is arbitrary; it was chosen because it is the largest plastic strain allowing the calculation of $d\sigma/d\epsilon$ before fracture for all the curves and the slopes of the curves become increasingly different at increasing strains. The results of these calculations are given in Table VI; they show a gradual increase in $d\sigma/d\epsilon$ for the specimens aged at 410°C and a less well

Table IV. Mechanical Property Measurements for 60% Au-40% Pt Alloys Aged at 510°C

Aging Time Hrs.	E 10^{-6} psi	PL 10^{-3} psi	FRAC 10^{-3} psi	Elastic Strain X 10^{3}	Plastic Strain X 10^{3}
0*	21.6	74	121	3.43	32.3
0.5	20.5	95	160	4.62	4.20
1*	19.2	96	162	5.03	4.05
5*	20.9	110	161	5.29	2.65
10*	21.4	110	169	5.19	2.98
20*	21.1	110	169	5.24	3.02
97.5*	21.6	109	166	5.09	2.98

E = Young's Modulus

PL = Initial yield point on stress-strain curve (proportional limit)

FRAC = Engineering fracture stress

* = Denotes average values for duplicate specimens

Table V. Mechanical Property Measurements for 60% Au-40% Pt Alloys Aged at 410°C.

Aging Time Hrs.	E 10^{-6} psi	PL 10^{-3} psi	FRAC 10^{-3} psi	Elastic Strain X 10^{3}	Plastic Strain X 10^{3}
0*	21.6	74	121	3.43	32.3
5	20.6	96	150	4.68	5.57
10	22.0	96	155	4.37	4.80
40	21.0	111	167	5.28	3.90
200*	20.8	102	160	4.90	3.04

E = Young's Modulus

PL = Initial yield point on stress-strain curve (proportional limit)

FRAC = Engineering fracture stress

* = Denotes average values for duplicate specimens

Table VI. Work Hardening Rates of 60% Au- 40% Pt Alloys Measured at $_{plastic} = 2.5 \times 10^{-3}$ for Various Aging Times and Temperatures.

Age Temperature (°C)	Age Time hours	$d\sigma/d\epsilon$ (psi) $\times 10^{-6}$
0*	0	4.8 (homogenized and quenched specimens)
410	5	10.1
410	10	12.0
410	40	14.4
410*	200	17.6
510	0.5	16.4
510	1	15.8
510	5	19.0
510*	10	18.3
510*	20	18.6
510*	97.5	17.7

* Average values for duplicate specimens.

defined increase for those aged at 510°C. The work-hardening rate of the flat portion of the stress-strain curve for the homogenized and quenched specimens was about 1.4×10^6 psi or 0.05 E, where E = 21 ± 1×10^6 psi, the average value for all 60% Au-40% Pt specimens tested. The work hardening rates at a plastic strain equal to 2.5×10^{-3} range from about 0.2E in the case of the homogenized and quenched specimens up to a constant value of about 0.85 E. The average value of Young's modulus for all specimens tested is 21 ± 1×10^6 psi.

A number of tensile tests were conducted on quenched specimens of the 20Au-80Pt alloy. This alloy always fractured while still in the elastic

region of the stress-strain curve. Fracture strengths were generally about 130,000 psi. No further mechanical properties tests were carried out on this alloy.

3. Metallographic Structure

The fractures occurring in the tensile specimens were examined optically. All fractures other than those in the homogenized and quenched 60 Au-40 Pt specimens were found to occur in the grain boundaries. The homogenized and quenched specimen fractured by ductile shear, as shown in Figs. 10 and 11. Figures 12, 13 and 14 are characteristic fractures of 60-40 alloys aged at 510°C for 1, 10 and 20 hours, respectively. A low magnification photograph of a characteristic fracture of the homogenized and quenched 20% Au-80% Pt allys is shown in Fig. 15. The surface irregularity of the fractures precludes high magnification views of the entire fractured surface, but single grain boundaries can be photographed with reasonable clarity. Figure 16 shows one side of a grain boundary fracture surface of a 60-40 specimen aged 10 hours at 510°C; precipitate on the fracture surface is clearly visible. A similar micrograph of a 60-40 alloy aged 200 hrs. at 410°C and fractured is shown in Fig. 17. Grain boundary precipitation occurs in both the 60-40 and 20-80 alloys during quenching from the homogenization temperature as shown in Figs. 18, 19a, and 19b, respectively. Figures 20 and 21 show the further growth of the phases forming at the grain boundary after aging a 60-40 alloy for 25 and 97.5 hours at 510°C, respectively.

An optical examination to determine the presence of slip within grains was made on the surface of tensile specimens which had been electro-polished before testing. Figures 22, 23, 24 and 25 show grain surfaces on the cylindrical specimen surface of a specimen that had been aged for 1.1 hours at

510°C. About one-third of the grains showed observable slip lines as shown in Figs. 22 and 23, however, observation of multiple slip was quite rare. The slipped grains were randomly distributed over the polished section, which was the central one-half inch of the gage section. Grains of the same specimen not having optically observable slip lines are shown in Fig. 24. Near the fracture, which occurred at one end of the polished section, rather coarse slip bands were observed within the grains. An example of this is shown in Fig. 25; coarse slip of this nature was not observed except in grains on the fracture surface.

Figure 26 shows coarse slip bands on a polished specimen that was tensile tested to fracture in the quenched condition. Slip bands of this appearance were observed in all grains in the polished region of the specimen.

D. DISCUSSION OF EXPERIMENTAL RESULTS

1. Structural Changes and the Work-Hardening Rate

The changes observed in the diffraction patterns during the sideband stages of the reaction agree quite well with previous x-ray investigations of the Au-Pt system.[6,7] Tiedema. et al[6] have shown that the intensity asymmetry evident in the sideband photographs is due to different amounts of the precipitating phases present in the alloy; their calculations showed that the intensity ratio between two symmetric (with respect to position) sidebands was in reasonable agreement with the amounts to the two phases present at equilibrium, as determined from the phase diagram.[13] For the 20-80 alloy, in which the Pt-rich phase is the major constituent at equilibrium, the high angle sideband is the most intense, since the Pt-rich modulation has a smaller lattice parameter than the quenched solution or the Au-rich equilibrium phase; from the Bragg relation it should be present at a higher angle. The converse holds true for the 60-40 alloy. The streaking which occurs in the x-ray photographs when the least intense sideband disappears has been observed by Tiedema. et al.[6] in a 20 Au-80 Pt single crystal after annealing for 1 hour at 600 °C, and [7] has been attributed to thin plates of the equilibrium incoherent precipitate. Later, van der Toorn showed by diffraction analysis that these streaks result from thin plates of precipitate; the habit plane is {100}. The present x-ray data shows λ to increase by a factor of about two from an initial value of 16 to 17 unit cell distances (a_o). There is a slightly greater increase before the loss of the least intense sideband in the 20-80 alloys than in the 60-40 alloys. Tiedema et al.[6] has calculated that $\lambda = 20.5a_o$ for an 20 Au-80 Pt single cyrstal aged 15 minuted at 600°C.

This is in very good agreement with the present data where $\lambda = 23.5a_o$ for a polycrystalline alloy aged under the same experimental conditions.

The gradual sharpening of the sidebands as the aging reaction progresses has been noted in previous investigations of both Au-Pt and Fe-Cu-Ni systems; it is attributed to a spectrum of wavelengths present in the alloy which becomes continually smaller as aging progresses, the calculated values representing the average wavelength of the structure. The lattice constant calculated from the main Bragg lines was found to be constant in the sideband stage of the reaction which is in agreement with earlier investigations.

The most unusual mechanical property characteristic observed in the present work is the very high work hardening rate, which occurs early in the aging treatments at 510 °C. A theory to explain this effect has been presented by Parker, Carpenter, and Zackay.[14] The structural model assumed for the theory is the one developed from the x-ray data: during the sideband stage of spinodal decomposition, the unstable fcc solution has a modulated lattice parameter along the three cube axis directions.

Before describing this theory it is worthwhile to point out the reasons why no conventional structural age hardening mechanism can be applied to this spinodal system.

Theoretical treatments of the deformation characteristics of age hardening alloys can be conveniently divided into two groups:

1) Theories that consider hard particles dispersed within a relatively ductile matrix exemplified by the work of Orowan[15] and that of Fisher, Hart, and Pry.[16] This model assumes that hard, incoherent precipitate particles intersecting an active slip plane cannot be sheared at small plastic strains by dislocations moving under an externally applied force. In order for

deformation to occur dislocations must pass between the particles, leaving loops around the particles. Since the matrix containing the incoherent hard particle dispersion is initially undeformed, the initial yield stress is low; the initial work hardening rate is high because the backstress on the slip plane is proportional to the number of dislocation loops around the unsheared particle. The high work rate in spinodally hardened gold platinum alloys suggests a similar mechanism, however for this model to apply dislocations must be able to pass between the hard particles. Fisher, et al.[16] have calculated that the shear stress necessary to force a dislocation between two obstacles on a slip plane is approximately:

$$\tau = \frac{3bN\, r^2 G}{R^3} \qquad (2)$$

where:

b = dislocation burgers vector

G = matrix shear modulus

r = particle radius

2R = mean center to center spacing of particles in the slip plane.

In the spinodal structure τ would be calculated by putting $r = R = \frac{1}{2}\lambda$. The maximum λ observed is about 40 a_o or 160 Å. To estimate the shear modulus of the Au-Pt alloy it is assumed Poisson's ratio is the mean of the values for the elements which are 0.39 and 0.42 for Pt and Au, respectively.[17] The slip system for the spinodal alloy has not been identified. However, it can reasonably be assumed to be $\{111\}\ \langle 1\bar{1}0\rangle$. The shear modulus, G, is given by

$$G = \frac{E}{2(1+\nu)} = \frac{21 \times 10^6}{2.8} = 7.5 \times 10^6 \text{ psi} \qquad (3)$$

The shear stress increment due to work hardening necessary to propagate the second dislocation further than one-half wavelength is about $3(5.6)\frac{G}{\lambda} = 7.9 \times 10^5$ psi. This corresponds to a tensile stress increment of about 1.6×10^6 psi. This model clearly cannot apply to the present case.

2) The other general class of age-hardening theories assumes the precipitate or preprecipitate particles are coherent with the matrix. When deformation takes place in these alloys shearing of the particles usually occurs, certainly when the particles are of less than about 200Å diameter,[12] which is the present case. It has also been observed that alloys having this type of deformation mechanism invariably show a large increase in yield point relative to the quenched supersaturated solid solution and the work hardening rate is about the same as that of a pure metal or solid solution; generally less than 0.1E.[12] There is no unified theory of deformation or work-hardening rate for alloys of this type. A number of theories have been developed for special cases and according to the most recent review (Kelly and Nicholson[12]) they all depend on the volume fraction of precipitate, which must have different properties than the matrix. There are at least two reasons why these theories cannot be applied to hardening by spinodal decomposition. First, it is difficult if not impossible to give a definition of precipitate volume fraction in a spinodally decomposing system, because after nucleation the whole crystal is composed of small scale composition fluctuations. This point of view is supported by all theoretical considerations of spinodal decomposition,[1-5] and there is no conclusive experimental evidence to the contrary. Second, the low work hardening rates observed experimentally in alloys of this type are in disagreement with the present data for gold-platinum.

For the theoretical treatment of work hardening simple slip is assumed. This assumption is well supported by the slip line observations described on Page 20. The slip system is assumed to be {111} $\langle 1\bar{1}0 \rangle$ type. In one dimension the modulation of the lattice parameter is given by

$$a = a_o + \frac{\Delta a}{2} \sin \Pi \frac{x}{(\lambda/2)} \tag{4}$$

where

a_o = lattice constant of quenched solution

Δa = maximum difference in lattice constant between gold-rich and platinum-rich regions.

The propagation of dislocations will cause strains by shearing a platinum-rich region over the adjacent gold-rich region. The passage of a single dislocation through the composition fluctuation will cause a shear strain of

$$\gamma = \frac{C(a \cdot y)}{2} \left(\frac{1}{\lambda}\right) \sin \Pi \frac{nb}{(\lambda/2)} \tag{5}$$

where C is the number of lattice constants per wavelength, where b is the burgers vector and y a unit vector in the slip direction. If n dislocations pass through the fluctuation, noting that $\lambda = Ca_o$ on the average, then

$$\gamma = \frac{\sqrt{2}\Delta a}{2a_o} \sin \Pi \left(\frac{2n}{\lambda'}\right) \tag{6}$$

where λ' is the wavelength in burgers vectors. The tensile stress, T, opposing the further propagation of dislocations through the lattice (assuming the Schmid factor = $\frac{1}{2}$ for polycrystalline fcc metals) is

$$T = \frac{\sqrt{2}\Delta a}{a_o} G \sin \left(\frac{2\Pi n}{\lambda'}\right) \tag{7}$$

and the total flow stress for the alloy in the plastic region is

$$\sigma_T = \sigma_{PL} + \frac{\sqrt{2\Delta a}}{a_o} G \sin\left(\frac{2\Pi n}{\lambda'}\right) \qquad (8)$$

where σ_{PL} is the stress at the experimentally observed proportional limit. An approximate calculation of Δa, which is unavailable from x-ray diffraction or thermodynamic measurements, on gold-platinum alloys can be made from x-ray measurements of spinodal decomposition in other alloys. Guinier[18] has pointed out that alloys exhibiting sidebands in the early stages of decomposition have in common a face-centered-cubic single phase at elevated temperatures which decomposes into two face-centered cubic conjugate equilibrium phases at lower temperatures, within the miscibility gap. These alloys, of which gold-platinum is one, may exhibit intermediate stages in the overall precipitation reaction in addition to the sideband stage, and the occurrence of other intermediate stages is related to the difference in lattice constants of the equilibrium cubic phases. For example, spinodal decomposition in iron-copper-nickel alloys begins with the sideband stage and then passes into a second intermediate stage during which two tetragonal phases with very small differences in lattice constants coexist. Following the tetragonal stage the equilibrium cubic phases appear; the cubic phases differ in lattice constant by less than 1%.[9] In gold-platinum alloys the sideband intermediate stage is the only one observed and the difference in cubic lattice constants is about 3%. Gold-nickel alloys have a difference between cubic lattice parameters of about 10%.[18] and it is very difficult to obtain even the initial modulated (sideband) intermediate stage in these alloys;[19] the most common decomposition mechanism in this case is discontinuous precipitation at the grain boundaries. It is reasonable to assume that the existence of the modulated structure depends on the strain-

energy associated with it; the strain energy will become larger as Δa becomes larger and the occurrence of intermediate stages beyond that of sidebands depends on the difference in atomic diameters of the constituent atoms. If the difference is too large the c/a ratio of the coexisting tetragonal phases will be too large for this stage to occur, and the cubic equilibrium phases appear directly. The maximum value of the cubic lattice constant modulation can be calculated from the measured lattice constants of the tetragonal phases for iron-copper-nickel alloys by assuming that the volume of the tetragonal cells is the same as the cubic modulations that preceded them. Hargreave's data give $a_o = 3.598\text{Å}$ for the copper-rich region and $a_o = 3.575\text{Å}$ for the copper-poor region so $\Delta a = 0.023\text{Å}$. The average lattice constant of the modulated structure is 3.586Å. It is assumed that the modulated (sideband), initial stage of spinodal decomposition in iron-copper-nickel and gold-platinum alloys is the same so Δa for gold-platinum alloys is

$$\Delta a_{\text{Au-Pt}} = \Delta a_{\text{Fe-Cu-Ni}}\left(\frac{\bar{a}_{\text{Au-Pt}}}{\bar{a}_{\text{Fe-Cu-Ni}}}\right) = 0.026\text{Å}$$

This calculation neglects differences in elastic moduli between the two systems, however a recent estimate[20] shows that they probably do not differ by more than about 15%, which is negligible for the present purpose.

An estimate of Δa for the gold-platinum system can also be made from the diffusion data of Bolk[21] and the activation energy for the spinodal reaction determined in the present work (to be discussed in a later section). Bolk has shown that the chemical diffusion coefficient in the gold-platinum system is concentration dependent; the diffusion coefficient is smaller at higher platinum concentrations. The temperature-independent part of the diffusion coefficient (frequency factor) decreases from about 9×10^{-2} for a

gold mol fraction of 0.8 to 4×10^{-6} cm^2/sec if the gold mol fraction is less than 0.08, for a diffusion couple of fine-grained pure platinum and gold. The phase diagram for the gold-platinum system[13] shows that at 500°C the compositions of the equilibrium phases within the miscibility gap are 79% gold and 1% gold. The spinodal compositions at 500°C are about 61% Au and 9% Au, thus the precipitation reaction in the 60 Au-40 Pt alloy occurs mainly by a redistribution of platinum atoms and will be limited by the slow diffusion rate in the platinum-rich regions, which approach pure platinum as the reaction progresses. The distance between the centers of gold- and platinum-rich regions is $\frac{1}{2}\lambda$. Atoms must move this distance to achieve equilibrium. Since Vegard's law is followed closely in this system, the fraction of this distance an average atom moves during aging is proportional to Δa for the aging cycle. The average distance moved is approximately $(Dt)^{1/2}$, where $D = D_o \exp(-Q/RT)$ cm^2/sec and t is the time in seconds at temperature T. Taking $D_o \cong 10^{-5}$ cm^2/sec and Q = 48 kcal/mol for 10 hours at 500°C, the average distance moved is one-quarter the distance between gold and platinum rich regions. The equilibrium difference between lattice constants of gold-rich and platinum-rich regions is 0.115Å; thus $\Delta a \cong 0.029$Å for 10 hrs. age at 500°C, in good agreement with the estimate from diffraction data. For gold-platinum alloys the maximum value of Δa is taken to be 0.026Å.

Assuming that the active slip planes in this type alloy are about 1μ apart, and using the previously calculated shear modulus of 7.5×10^6 psi a stress-strain curve for a spinodally hardened 60-40 alloy having a wavelength of 40b has been calculated. The resulting points are shown in Fig. 27 with the experimental curve for the alloys aged 10 hrs. at 510°C. The agreement is quite good.

From Eq. (8) it can be seen that the trigonometric term determines the form of the stress-strain curve, causing the work-hardening rate to be high and Δa, the maximum difference in lattice parameter between gold-rich and platinum-rich modulations, determines the absolute magnitude of the internal stress, neglecting variations of the shear modulus, G, with composition. It was assumed above that in the early stages of the transformation Δa also increases from some value close to zero in the quenched alloy up to a maximum when coherency is lost and a value for 10 hrs. aging was calculated. The theoretical treatments of spinodal decomposition due to Hillert and Cahn also predict this behavior. The lower work-hardening rates of the tensile specimens aged for very short times at 510°C suggest this is occurring; to examine the problem further, tensile tests were made on specimens aged at 410°C. The work-hardening rates at 0.25% plastic strain of these specimens increased in a gradual way from 0.5E to about 0.85E for aging times of 5 up to 200 hrs. X-ray diffraction showed the average wavelength to increase from about 20 to 24 lattice constants during the aging period. The sidebands were broad, indicating a spectrum of wavelengths present, as in the early stages of aging at higher temperatures. Consideration of Eq. (8) shows that for fixed plastic strain (i.e., n constant) an increase in λ will cause a decrease, rather than an increase in work-hardening rate. The observed increase in work-hardening rate with time at 410°C is very strong evidence that a increases with aging time at a rate large enough to predominate over the small increases observed in λ.

2. Fracture Characteristics

The experimental results show that fracture in all specimens hardened by spinodal decomposition is through the grain boundaries. The microstructural investigation showed that in all quenched specimens a small amount of

precipitate is present in the grain boundaries and the amount of precipitate increases upon aging.

The microhardness of most alloys was measured for comparison with the data of Tiedema et al.[6] and van der Toorn.[7] The same general behavior was found, an increase with aging time in the early stages followed by a small decrease (Table VII). The hardness of the grain-boundary regions was less than that of central portions of the grains, but a quantitative comparison cannot be made because the hardness indenter is wider than the grain boundaries. The softness of the grain boundaries relative to the grains is opposite to the usual observation in which intergranular brittle-type fracture is attributed to a brittle, hard intermetallic or impurity-compound film in the boundaries.

An experimental investigation of the grain-boundary regions for impurities or differences in composition from the grains themselves was conducted with an electron-beam microprobe. Particular attention was given to silicon, since these alloys were melted in zirconium silicate crucibles and platinum silicides are well-known brittle intermetallic compounds. No trace of silicon was found; the grain boundary regions showed no significant difference in composition from the grains themselves, within the experimental limits of the method. It is thought that softer material in the boundaries is prevented from deforming by the constraint of the surrounding hard grains. The nearly constant small plastic tensile elongation of specimens in the hardened condition, compared to metallographic evidence that the amount of grain-boundary precipitate is increasing with aging time, supports this reasoning. It is evident that in this case the brittle-type fracture through the boundaries is due to precipitation in the grain boundaries of small amounts of soft, nearly

Table VII. Variation of Hardness with Aging Treatment for Gold-Platinum Alloys

80 Pt - 20 Au Alloy							
	(515°C)			(685°C)			
Aging Time*	0	5	60	0	5	10	15
H_V**	406	525	572	406	525	585	521

40 Pt - 60 Au Alloy							
	(510°C)						
Aging Time	0	30	60	120	130	600	1200
H_V	314	493	483	493	514	514	464

* Expressed in minutes

** Vickers hardness, 25 gram load

Aging temperatures in parenthesis

equilibrium phase material, which is much weaker than the hard grains. To further substantiate the conclusion that the equilibrium two phase alloy is soft and ductile, several 60 Au-40 Pt specimens were annealed at 900°C until a large grained structure of the two equilibrium phases was obtained.

The microstructure of such a specimen is shown in Fig. 28. The stress-strain curves for these alloys (Fig. 29) were characteristic of face-centered cubic metals; low yield stress and work-hardening rate, and strain-to-fracture greater than 10%.

3. Increase in Yield Stress

It is apparent from the results of mechanical properties experiments that the yield stress, taken here to be the same as the proportional limit, is increasing with aging time. Cahn[22] has theoretically analyzed the increase in yield stress for an alloy undergoing spinodal decomposition. It is of interest to compare the observed increases in yield strength with this theory, because it is the first attempt to analyze the yield stress increase resulting from spinodal decomposition. The contributions to the forces on a stationary dislocation in equilibrium with its surrounding (i.e., before the application of an external force causing movement of dislocations) from the tessellated stress field caused by the periodic variation in lattice constant are shown to be predominant, compared to other contributions such as the variation of dislocation line tension with the microscopic composition inhomogenieties. For the (111) $[1\bar{1}0]$ slip system in a face-centered cubic alloy, Cahn has assumed a string model for the dislocation and calculated equilibrium shapes for both edge and screw dislocations in the presence of the tessellated stress field. Two cases are found:

1) If the dislocation is very flexible, it can curve around all the energy hills of the stress field and loop between them. This corresponds to Orowan hardening, discussed above.

2) If the dislocation is less easily bent, it must remain nearly

straight and shear the composition inhomogenieties when moving under the influence of an external stress. Cahn assumes a sinusoidal composition fluctuation (which is equivalent to a sinusoidal lattice parameter fluctuation in the gold-platinum system) of the form

$$c - c_o = A \sin \frac{2\pi x}{\lambda} \tag{9}$$

where

c = composition at position x in the alloy

c_o = average alloy composition

A = amplitude of the composition fluction, which depends on λ

λ = wavelength of the fluctuation, in lattice parameters

x = distance along cube axis

It is shown that if $A\eta bE/(2\pi L) > 1$ then case (1), Orowan hardening should take place. If $A\eta bE/(2\pi L) < 1$ the dislocation is nearly straight and shearing of composition fluctuations should occur. Now, in the expression

$$\frac{A\eta bE}{2\pi L}, \tag{10}$$

E is Young's modulus, b is the burgers vector of the active slip system, L is the self-energy of the dislocation (taken to be Gb^2) and $\eta = d\ell na/dc$ where a is the lattice constant. In Eq. (10) the product $A\eta$ is the local lattice strain resulting from the composition fluctuation. This can be seen in the following way:

$$\frac{d\ell na}{dc} = \frac{1}{a}\frac{da}{dc} = \frac{1}{a}\frac{\Delta a}{\Delta c}$$

for small fluctuations, to which Cahn restricts his theory. Now Δa is the difference in lattice constants between gold-rich and platinum-rich regions,

for the composition fluctuation Δc and a is the average lattice parameter. From Eq. (9) A is the composition amplitude of the fluctuation, over the mean composition, c_o, therefore $A = \frac{1}{2} \Delta c$. Then

$$A\eta = \frac{\Delta a}{2a_o}, \tag{11}$$

which is the same strain parameter used in the discussion of work-hardening above. Now the criterion for shearing or non-shearing of composition fluctuations becomes

$$\frac{\Delta a E b \lambda}{4\Pi a_o L} = \frac{\Delta a E \lambda}{4\Pi a_o G b} \tag{12}$$

Using the same values for these parameters that were used in the discussion above,

$$\frac{\Delta a E \lambda}{4\Pi a_o G b} = \frac{(.029)(21X10^6)(40b)}{4\Pi(4.015)(7.5X10^6)(6)} \cong 6 \times 10^{-3} < 1,$$

indicating that dislocations are nearly straight and shearing of composition fluctuations will occur during deformation. This is in agreement with the conclusions reached in the discussion of work-hardening above. For this case the applied stress necessary to cause yielding is given as

$$\sigma = \frac{(A\eta)^2 E^2 \lambda}{6\Pi \sqrt{6}\ Gb} \tag{13}$$

for screw dislocations, and

$$\sigma = \frac{(A\eta)^2 E^2 \lambda}{2\Pi \sqrt{2}\ Gb} \tag{14}$$

for edge dislocations.

It is seen that screw dislocations can move more easily. The experimental results show that the yield stress is about 10^5 psi for a 60Au-40Pt with a wavelength of 40b (corresponding to an aging treatment of 10 hrs

at 510°C). Substituting the values obtained earlier into Eq. (13), we have

$$\sigma = \frac{\left(\frac{.029}{8}\right)(21\times10^6)^2(40)}{6\Pi\sqrt{6}\,(7.5\times10^6)} \cong 600 \text{ psi},$$

a calculated stress much below the experimental value. For edge dislocations the calculated yield stress is about 2,800 psi, still far below the observed value.

It may be objected that the value of Δa, 0.026Å, calculated above is too low, causing an anomalously low calculated yield stress. However, assuming a yield stress of 10^5 psi and using Eq. (13), the value of Δa required to give a yield stress equal to the observed one can be calculated. This was done, and the required $\Delta a = 0.35$Å. This is too high to be physically realistic. The maximum permissible Δa is 0.115Å, the difference in lattice constants between the equilibrium phases at 500°C. Thus the value of Δa used above is not the cause of the discrepancy. Cahn has stated that his theory is the equivalent, for spinodal systems, of the Mott and Nabarro theory of hardening by long-range coherency stresses in nucleation and growth age-hardening systems. It is probable that the discrepancy between theory and experiment here results from either short-range coherency strains (not taken into account) or the way in which the long-range coherency stresses were averaged to arrive at Eqs. (13) and (14). The problem of averaging long range stress fields in cyrstals is a cause of uncertainty in applications of the theory of Mott and Nabarro, in cases where it is applicable.

4. Kinetics and Temperature Dependence of the Reaction Rate

The side-ways growth of a plate-type precipitate follows a rate equation of the form[10]

$$\ell^m - \ell_0^m = k(t-t_0) \qquad (15)$$

where ℓ = plate thickness at time t

ℓ_0 = plate thickness on formation

t = reaction time reckoned from t_0

t_0 = time of first measurement

k = rate constant

with m = 2.

Assuming that $\ell_0 = t_0 = 0$, the value of m can be calculated from the slope of a plot of log λ vs log t, such as Figs. 6 and 7 if k is independent of time. The slope was calculated for the "steady-state" linear portion of the curves so k is independent of time within this range. The value of m desired here is the reciprocal of the slope of the least squares equations given in Table III. Values of m for Au-Pt alloys are given in Table VIII.

Hillert has calculated m values in this way for a number of spinodal alloys in the Fe-Cu-Ni systems and finds that m always is between 4 and 5. The present data for the 60-40 alloy agree quite well with this value, but the 20-80 alloys are too low. Greenwood[23] has assumed a diffusion controlled coalescence model for spheres and derived an equation of the same form as Eq. (15) with m = 3, a value in much better agreement with the latter. Evidently the geometric arrangement of precipitate in the two Au-Pt alloys studied is somewhat different with the 60-40 alloys very similar to the arrangement in Fe-Cu-Ni spinodal alloys. It seems reasonable that small sinusoidal composition fluctuations could be considered as coalescing spheres in either case. The present x-ray data are not sufficient to deduce whatever difference there may be between the two alloys.

Table VIII. Values of m in Eq. (15) Calculated from Wavelength Kinetics Measurements

Alloy	Temperature	m
20-80	502	3.13
20-80	552	3.33
20-80	602	3.12
60-40	502	4.8
60-40	552	5.0
60-40	602	4.5

It is useful to calculate the temperature dependence of the spinodal reaction and to compare the result with what is known of the diffusion rate temperature dependence in this system. The usual assumption that the process can be represented by an Arrhenius-type equation is made:

$$r = A\, t\, e^{-Q/RT} \qquad (16)$$

where r = reaction rate determined by some convenient experimental method

A = temperature independent constant depending upon structure

t = time since beginning of measurements

Q = activation energy, kcal/mol

R = gas constant

T = absolute temperature, °K

The experimental results of sideband measurements vs time have been used to calculate a value of Q for each alloy investigated over the temperature range 500 to 600°C. For each alloy it has been assumed that r and A are constant within the linear portion of the wavelength time curves (Figs. 6 and 7).

Equation (16) can be written as

$$\log t = \log\left(\frac{r}{A}\right) + \frac{Q}{2.3R}\left(\frac{1}{T}\right) \qquad (17)$$

so that the slope of a curve of log time vs T^{-1} will give the activation energy. The left side of Eq. (17) was chosen as the time required for λ to reach $25a_o$, which is well within the linear portion of the kinetics curves. Equation (17) is plotted in Fig. 30 for both alloys investigated. Values of Q calculated are 48.9 and 47.4 kcal/mol for 20-80 and 60-40, respectively. These values are not significantly different so Q appears to be invariant within the spinodal region. This result agrees with Hillert et al.[10] who found Q invariant within the spinodal region of the Fe-Cu-Ni system.

Bolk[21] has investigated the Kirkendall effect in the Au-Pt system and calculated activation energies for diffusion using three-layer diffusion couples in the temperature range 926 to 1055°C. The results are given in Table IX.

Table IX. Activation Energies for Chemical Diffusion in Au-Pt

	Couple 1	Couple 2	Couple 3
Q kcal/mol	50.4 ± 5.2	55.2 ± 2.6	46.5 ± 5.3

Couple 2 is Au/Pt/Au with a Pt grain size of about 3 mm; couple 1 is the same except the Pt grain size is less than 0.1 mm. Couple 3 is Au/Alloy/Au; the alloy composition is 73.5 at-% Au, and its grain size is about equal to that of Pt in Couple 1. Bolk has attributed the difference in Q to variation in grain size. Q calculated here agrees well with the values of Couples 1 and 3, and is related to a process occurring within the grains, therefore

presumably independent of grain-boundary effects. The reason for Bolk's discrepancy is not apparent.

In Eq. (16) all the temperature dependence of the reaction rate is included in Q; a better approach to the calculation of Q takes into account the temperature dependence of the free-energy change for the precipitation reaction. Then the rate equation has the form

$$r = A\, t\, \Delta F(T) e^{-Q/RT} \qquad (18)$$

Since $|\Delta F(T)|$ becomes larger as T decreases and $\exp(-Q/RT)$ becomes smaller, inclusion of the free energy correction will give an apparent activation energy larger than the value calculated above. The thermodynamic model of van der Toorn, et al.[24] is commonly used to estimate $\Delta F(T)$ but has recently been checked by computer methods[25] and found to be in serious error. According to Hillert[10] the free energy term in Eq. (18) can be regarded as a decrease in interfacial energy accompanying the growth in wavelength of the structure and Becker's[26] model of coherent interfaces can be used to estimate $\Delta F(T)$. According to this model ΔF is proportional to the square of the width of the miscibility gap, which varies with temperature. The variation of gap width with temperature was measured from the phase diagram of Tiedema, et al.[6] whose data extends down to 500°C. The calculated correction turned out to be less than 1 kcal/mol, which is negligible for the present purpose. It is concluded that diffusion is the rate determining process for growth of the spinodal structure in the alloys investigated. This conclusion agrees with Hillert's results on Fe-Cu-Ni spinodal alloys, the only other spinodal system in which the rate-determining process has been investigated.

CONCLUSIONS

The size of the structural modulations induced in 60% Au-40% Pt and 20% Au-80% Pt alloys have been determined to have average wavelengths between about 20 and 40 lattice constants by x-ray diffraction methods. The temperature dependence of the reaction rate has been determined and found to agree with that of substitutional diffusion in this alloy system.

It has been unequivocally demonstrated that spinodal decomposition is an effective strengthening mechanism in these alloys. The most unusual mechanical property changes are a very high work-hardening rate and small plastic elongation. A theory has been proposed to explain the high work-hardening rate; the agreement between theory and experiment is quite good. The intergranular brittle-type fracture has been attributed to the presence of small amounts of nearly equilibrium soft precipitate in the grain boundaries.

ACKNOWLEDGEMENT

This work was performed under the auspices of the United States Atomic Energy Commission. I would especially like to express my appreciation for the encouragement and guidance of Professor Earl Parker throughout this work. The author is particularly indebted to Mr. R. L. Brady and the Engineering Test Section (Livermore Laboratory), who performed the difficult and tedious tensile tests necessary for this investigation, to Dr. Azziz Ahmadieh for assistance with metallographic and microhardness investigations and to Dr. Eugene Huffman for chemical analysis of the alloys. He would like to express his appreciation to George Georgakopoulos and George Gordon for performing the microprobe investigations and to others whose stimulating discussions and assistance were very helpful, particularly Drs. V. F. Zackay and Kurt Kennedy, and David E. Porter.

REFERENCES

1. G. Borelius, Ann. Physik, 28, 507 (1937).
2. G. Borelius, Arkiv. Mat. Astron., 32A, 1 (1944).
3. M. Hillert, Acta Met., 9, 525 (June 1961).
4. J. W. Cahn, Acta Met., 9, 795 (Sept. 1961).
5. J. W. Cahn, Acta Met., 10, 179 (March 1962).
6. T. J. Tiedema, J. Bouman, and W. G. Burgers, Acta Met., 5, 310 (June 1957).
7. L. J. van der Toorn, Acta Met., 8, 715 (Oct. 1960).
8. V. Daniel and H. Lipson, Proc. Roy. Soc. A., 181, 368 (1943); Proc. Roy. Soc. A., 182, 378 (1944).
9. M. E. Hargreaves, Acta Cryst., 2, 259 (1949); 4, 301 (1951).
10. M. Hillert, M. Cohen, and B. L. Averbach, Acta Met., 9, 536 (1961).
11. E. Biedermann and E. Kneller, Z. Metallk., 47, 289, 760 (1956).
12. A. Kelley and R. B. Nicholson, "Precipitation Hardening," 10, No. 3 of Progress in Materials Science, Ed. Bruce Chalmers, Pergamon Press (1963).
13. A. S. Darling, R. A. Mintern, and J. C. Chaston, J. Inst. Metals, 81, 125 (1952-1953).
14. E. R. Parker, R. W. Carpenter, and V. F. Zackay, "Decomposition Reactions in Gold-Platinum Alloys and Their Effects on Strength and Fracture Characteristics," International Journal of Fracture Mechanics (in press).
15. E. Orowan, "Symposium on Internal Stresses in Metals and Alloys," Inst. of Metals (1951).
16. J. C. Fisher, E. W. Hart, and R. H. Pry, Acta Met., 1, 336 (1953).

17. J. Friedel, Dislocations, (Pergamon Press, 1964) p. 456.

18. A. Guinier, "Heterogeneities in Solid Solutions" in Solid State Physics, Advances in Research and Applications, Vol 9, F. Sietz and D. Turnbull, eds. (Academic Press, 1959).

19. R. M. Fisher and J. D. Embury, Electron Microscopy 1964; Vol. A, Proceedings of the Third European Regional Conference, Prague (1964).

20. S. D. Dahlgren, private communication.

21. A. Bolk, Acta Met, 9, 632 (1961).

22. J. W. Cahn, Acta Met, 11, 1275 (1963).

23. G. W. Greenwood, Acta Met, 4, 243 (1956).

24. L. J. van der Toorn and T. J. Tiedema, Acta Met, 8, 711 (1960).

25. D. de Fontaine and J. E. Hilliard, Acta Met, 13, 1019 (1965).

26. R. Becker, Z. Metallkunde, 29, 245 (1937).

FIGURE CAPTIONS

Fig. 1 Phase diagram of gold-platinum alloy system showing spinodal curve. The shape of the free energy vs composition curve (for the meta-stable solid solution) at temperature T_1, is shown in the lower figure. The relationship of the free-energy curve to the spinodal curve is shown by the vertical lines.

Fig. 2 Schematic diagram of experimental apparatus for homogenization and quenching alloy specimens.

Fig. 3 Epoxy Resin bonded tensile grips shown disassembled, and assembled, with fractured specimen in mounting jig.

Fig. 4 (a,b) X-ray diffraction photographs of 60Au-40Pt alloy specimens aged for increasing times at 600°C, showing side bands.

1) Homogenized and quenched, no age.
2) Aged 1 minute. The large irregular light spot between (420) and (422) is an artifact formed during developing.
3) Aged 3 minutes.
4) Aged 9 minutes.
5) Aged 15 minutes.
6) Aged 21 minutes.
7) Aged 1 hour.

Fig. 5 (a,b) X-ray diffraction photographs of 20Au-80Pt alloy specimens aged for increasing times at 600°C, showing side bands.

1) Homogenized and quenched, no age.
2) Aged 1 minute.
3) Aged 3 minutes.
4) Aged 9 minutes.
5) Aged 15 minutes.

6) Aged 21 minutes.

7) Aged 1 hour.

Fig. 6 Average wavelength (in lattice parameters) vs isothermal aging time for 20Au-80Pt alloys (plotted logarithmically).

Fig. 7 Average wavelength (in lattice parameters) vs isothermal aging time for 60Au-40Pt alloys (plotted logarithmically).

Fig. 8 Stress-strain characteristics for 60Au-40Pt alloys aged at 510°C.

Fig. 9 Stress-strain characteristics for 60Au-40Pt alloys aged at 410°C.

Fig. 10 Shear type ductile fracture in homogenized and quenched 60Au-40Pt alloy (32X).

Fig. 11 Ductile fracture surface in homogenized and quenched 60Au-40Pt alloy (32X).

Fig. 12 Intergrannular brittle-type fracture in 60Au-40Pt alloy aged 1 hour at 510°C (32X).

Fig. 13 Intergrannular brittle-type fracture in 60Au-40Pt alloy aged 10 hours at 510°C (32X).

Fig. 14 Intergrannular brittle-type fracture in 60Au-40Pt alloy aged 20 hours at 510°C (32X).

Fig. 15 Macroscopic view of intergrannular fracture in 20Au-80Pt alloy, homogenized and quenched. (32X).

Fig. 16 Grain boundary fracture surface showing precipitate in 60Au-40Pt alloy aged 10 hours at 510°C (1000X).

Fig. 17 Grain boundary fracture surface in 60Au-40Pt alloy aged 200 hours at 410°C (1000X).

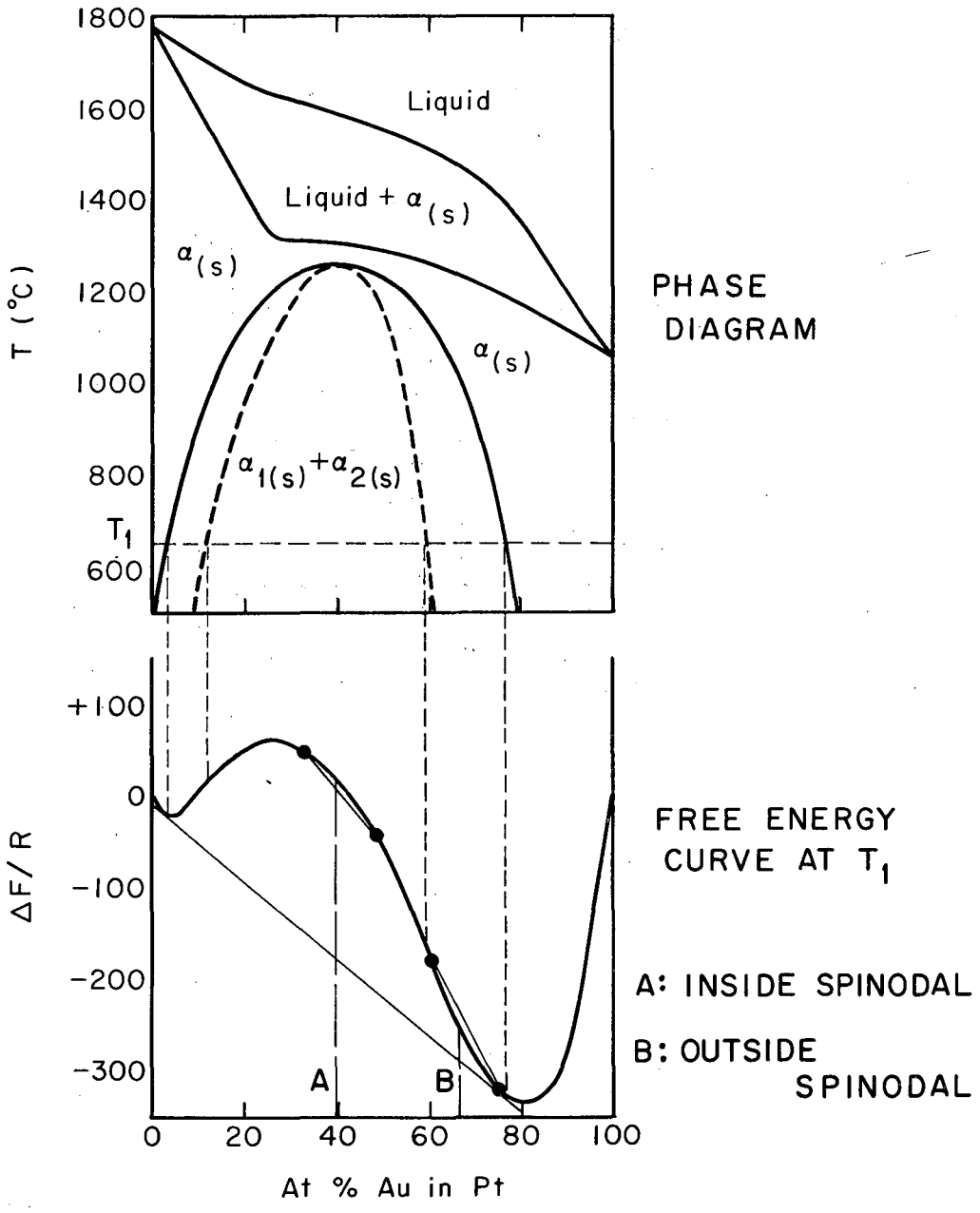
1800
1600
1400
1200
1000
800
T1
600
T (°C)
Liquid
Liquid + α(s)
α(s)
α(s)
α1(s)+α2(s)
PHASE DIAGRAM
+100
0
-100
-200
-300
ΔF/R
A
B
0
20
40
60
80
100
At % Au in Pt
FREE ENERGY CURVE AT T1
A: INSIDE SPINODAL
B: OUTSIDE SPINODAL
MUB-7533

Fig. 1

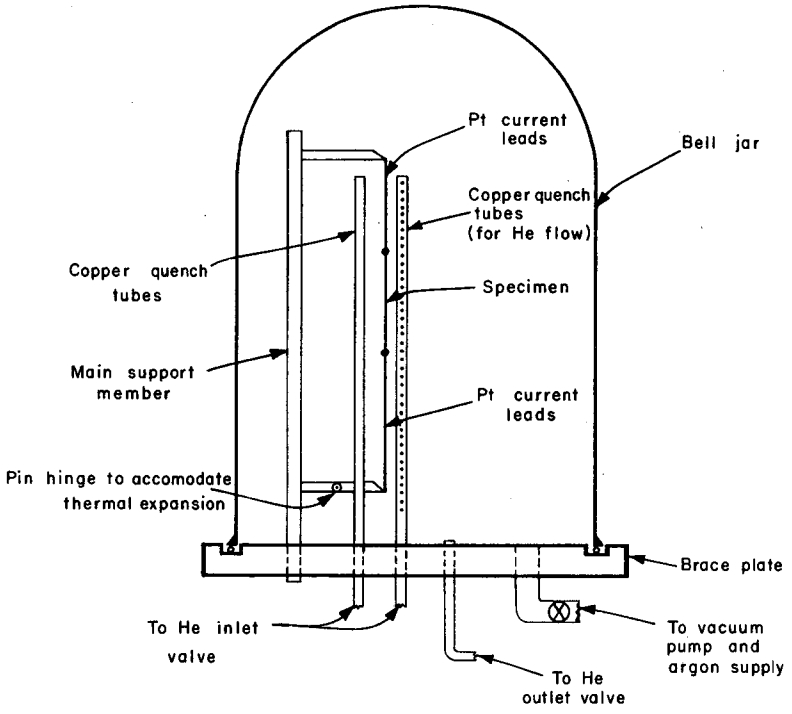
Pt current leads
Bell jar
Copper quench tubes (for He flow)
Copper quench tubes
Specimen
Main support member
Pt current leads
Pin hinge to accomodate thermal expansion
Brace plate
To He inlet valve
To vacuum pump and argon supply
To He outlet valve
MU-37190

Fig. 2

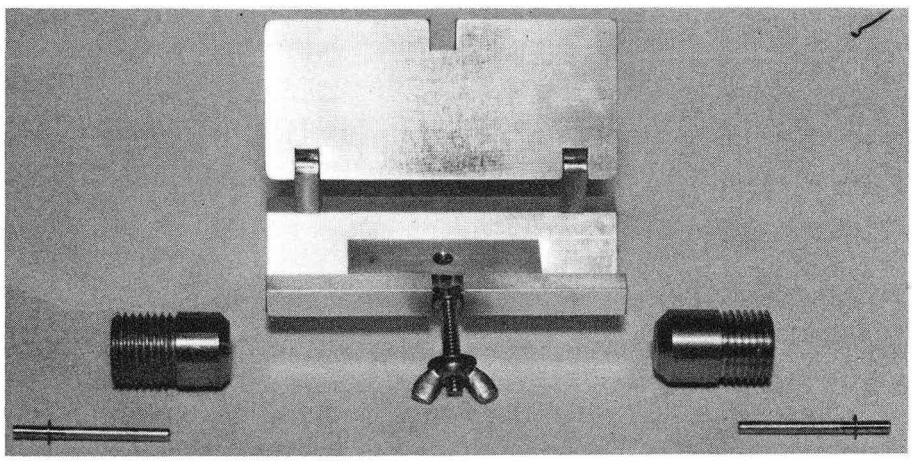

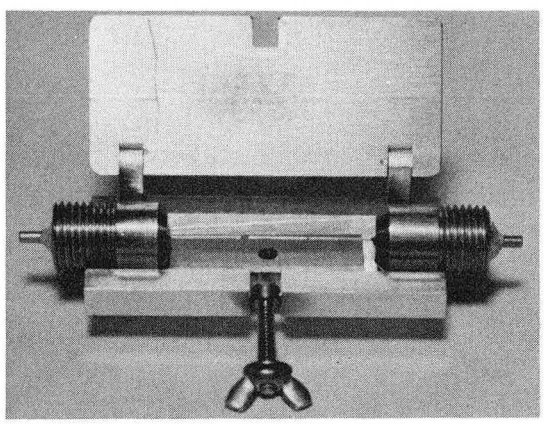

ZN-5786

Fig. 3

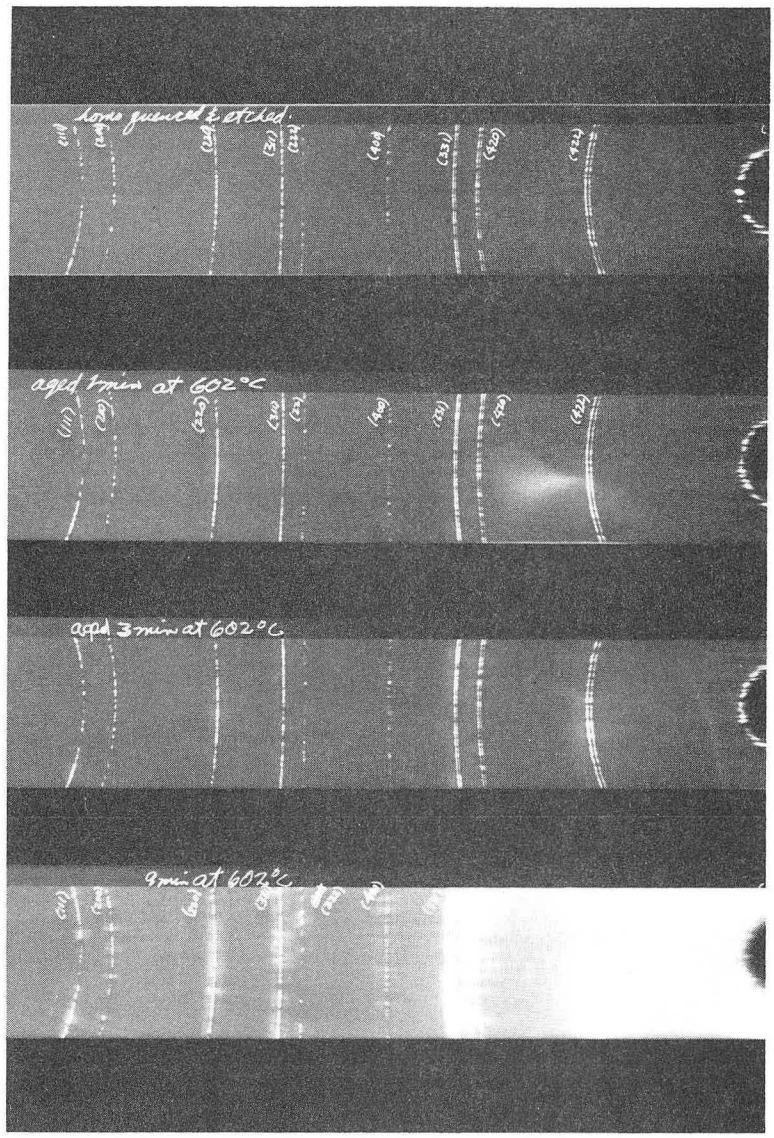

ZN-5787

Fig. 4a

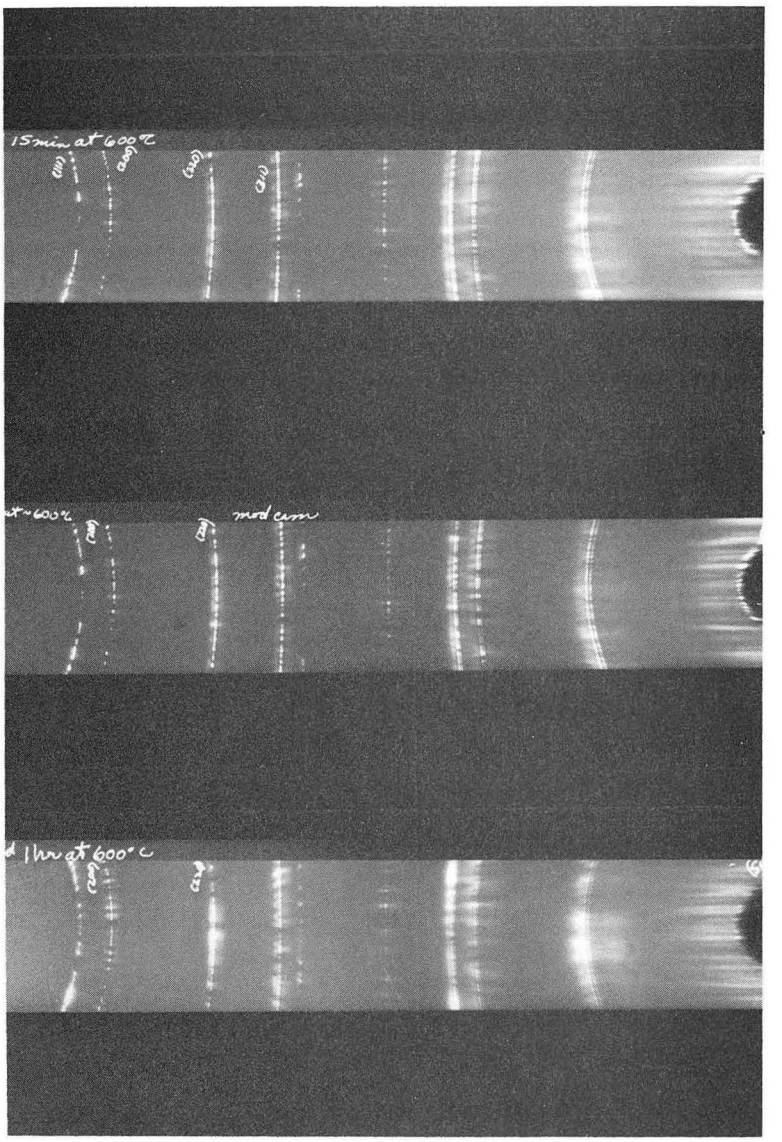

ZN-5788

Fig. 4b

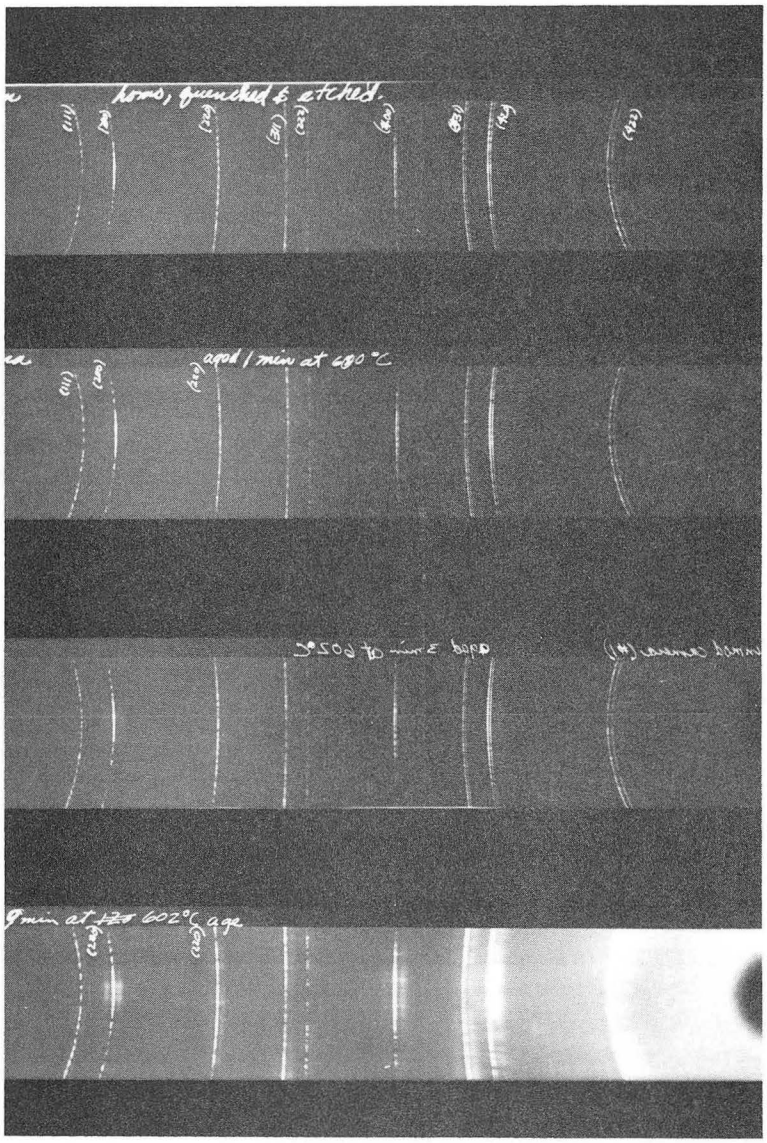

ZN-5789

Fig. 5a

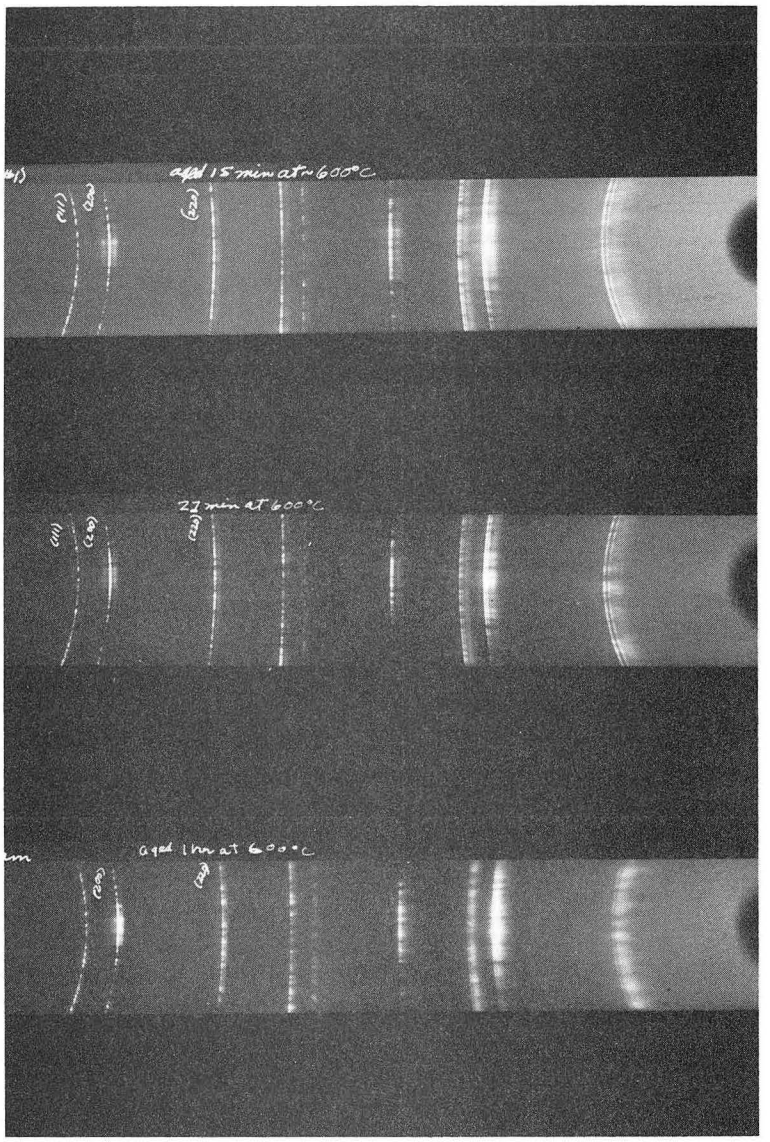

ZN-5790

Fig. 5b

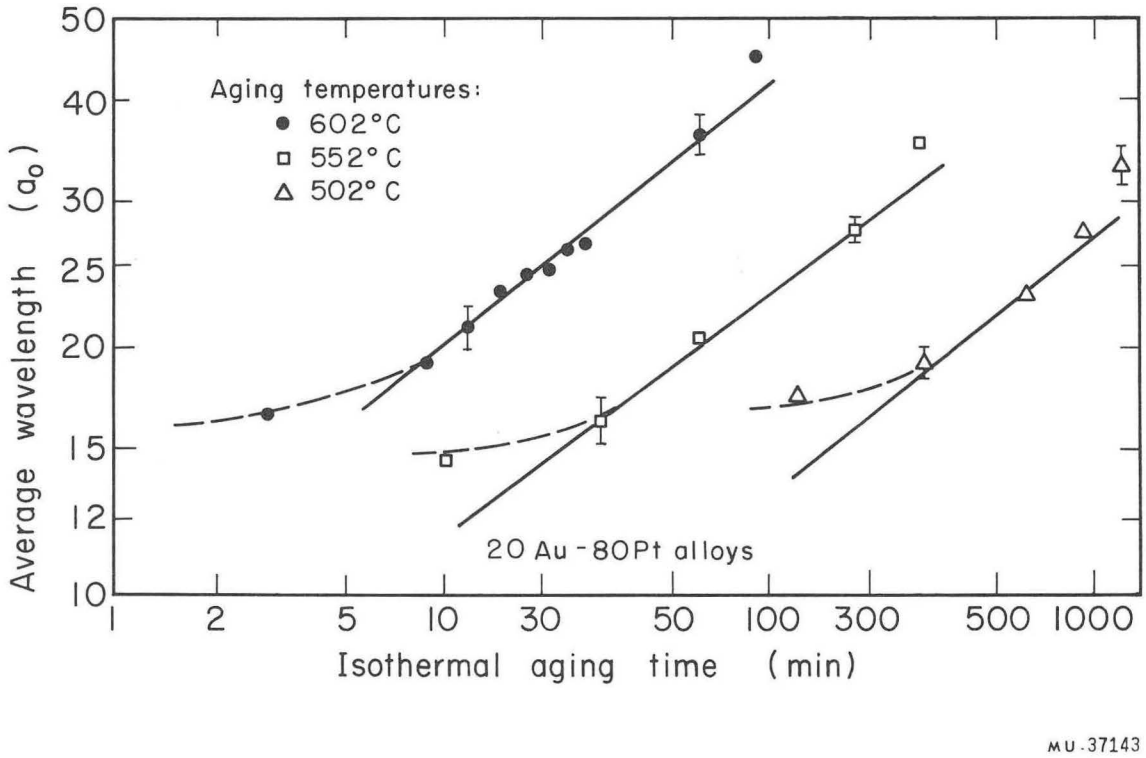
Aging temperatures:
602°C
552°C
502°C
20 Au-80Pt alloys
Average wavelength (a_o)
Isothermal aging time (min)
50
40
30
25
20
15
12
10
1
2
5
10
30
50
100
300
500
1000
MU-37143

Fig. 6

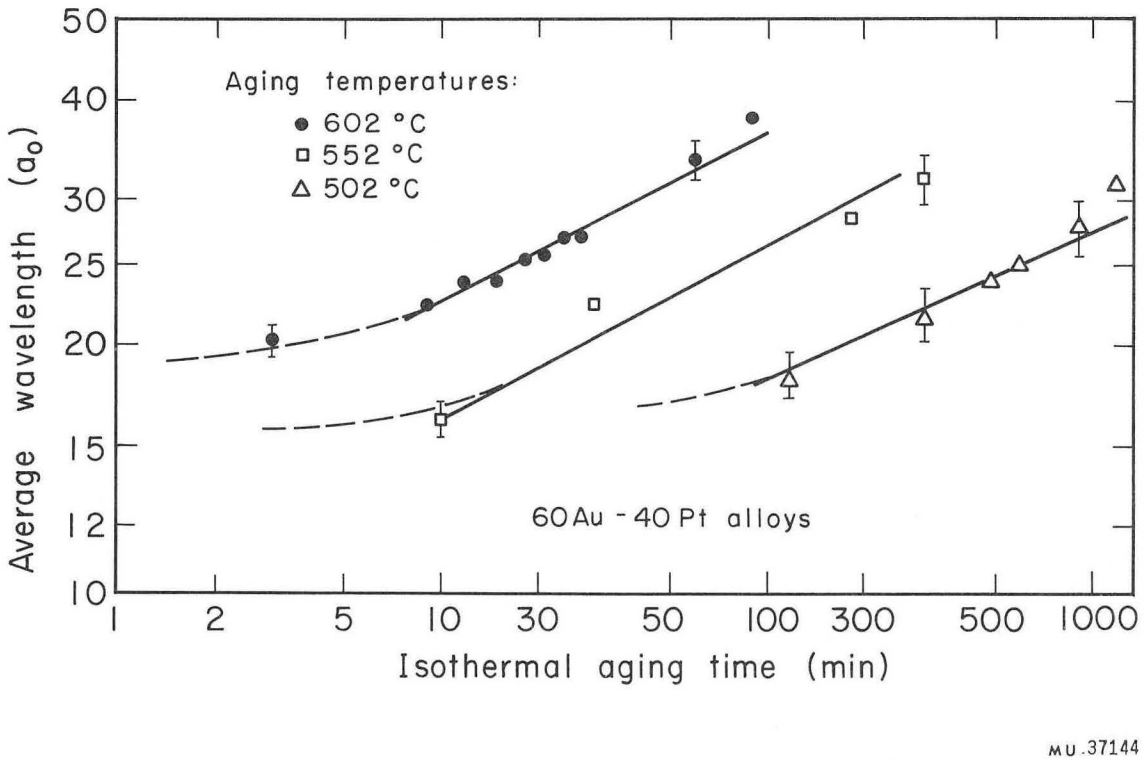
Aging temperatures:
602 °C
552 °C
502 °C
60Au - 40Pt alloys
Average wavelength (a_o)
Isothermal aging time (min)
50
40
30
25
20
15
12
10
1
2
5
10
30
50
100
300
500
1000
MU.37144

Fig. 7

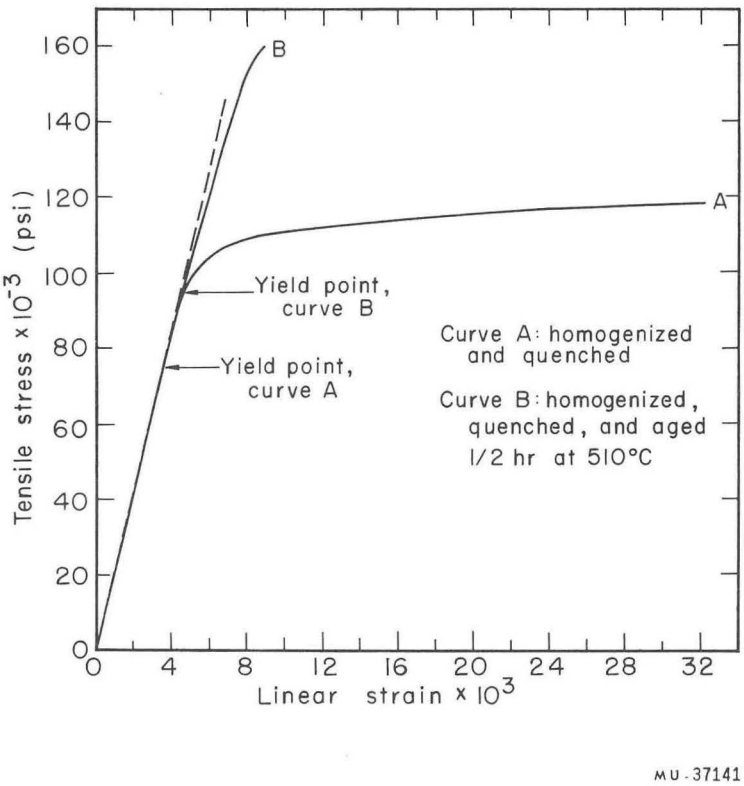
160
140
120
100
80
60
40
20
0
0
4
8
12
16
20
24
28
32
Tensile stress x 10^-3 (psi)
Linear strain x 10^3
B
A
Yield point, curve B
Yield point, curve A
Curve A: homogenized and quenched
Curve B: homogenized, quenched, and aged 1/2 hr at 510°C
MU-37141

Fig. 8

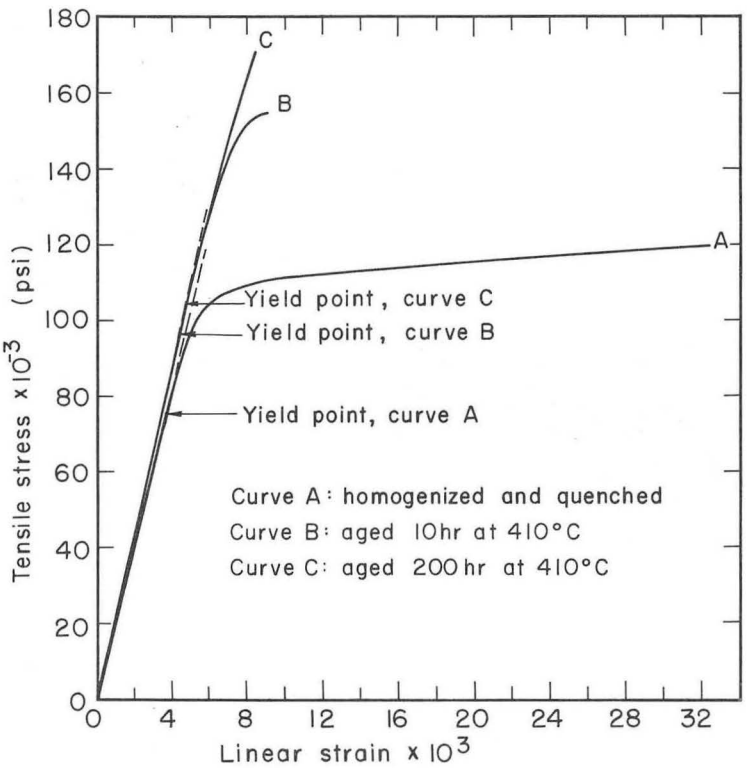
180
160
140
120
100
80
60
40
20
0
0
4
8
12
16
20
24
28
32
C
B
A
Yield point, curve C
Yield point, curve B
Yield point, curve A
Curve A: homogenized and quenched
Curve B: aged 10hr at 410°C
Curve C: aged 200 hr at 410°C
Tensile stress x10^{-3} (psi)
Linear strain x 10^{3}
MU-37142

Fig. 9

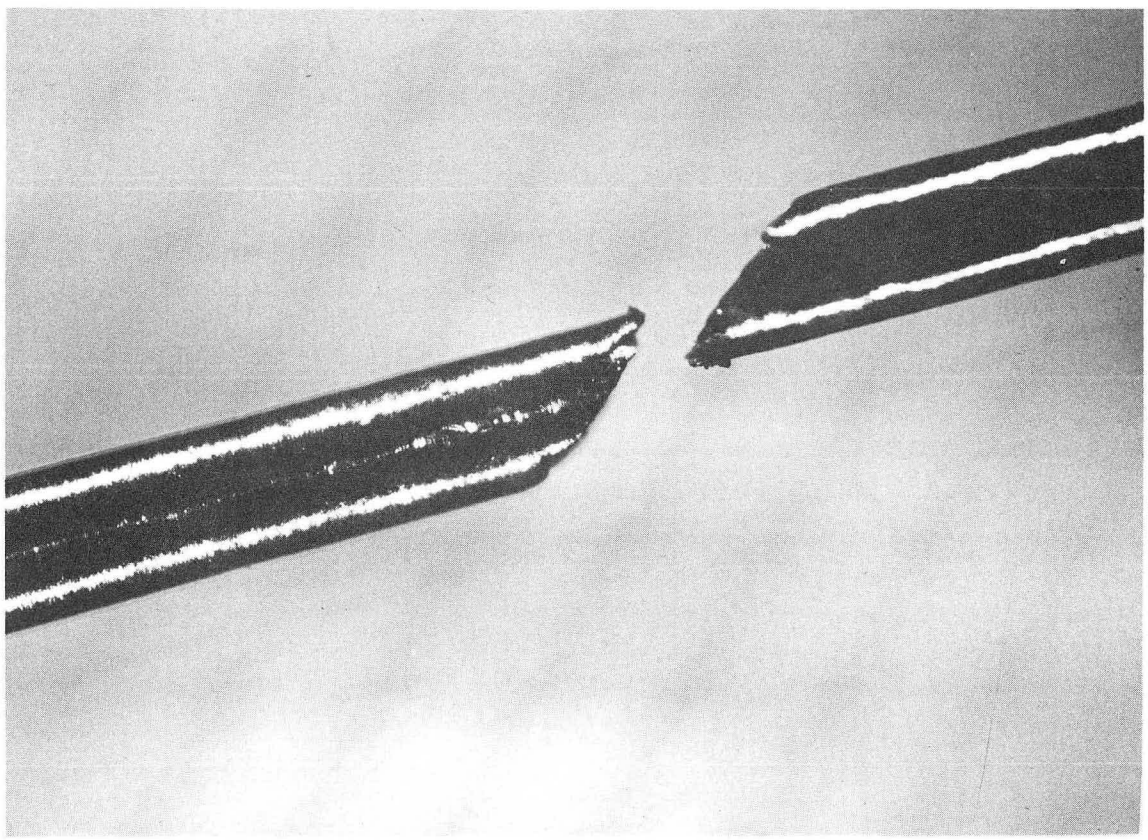

ZN-5240

Fig. 10

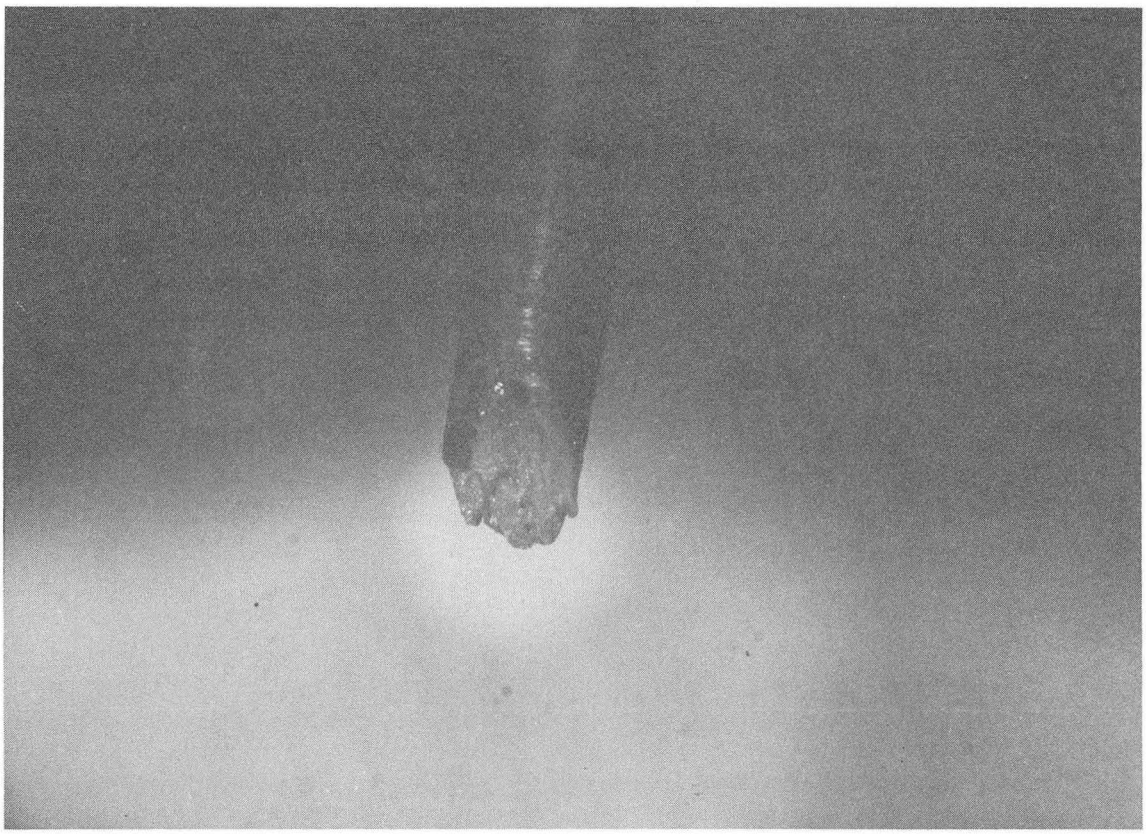

ZN-5791

Fig. 11

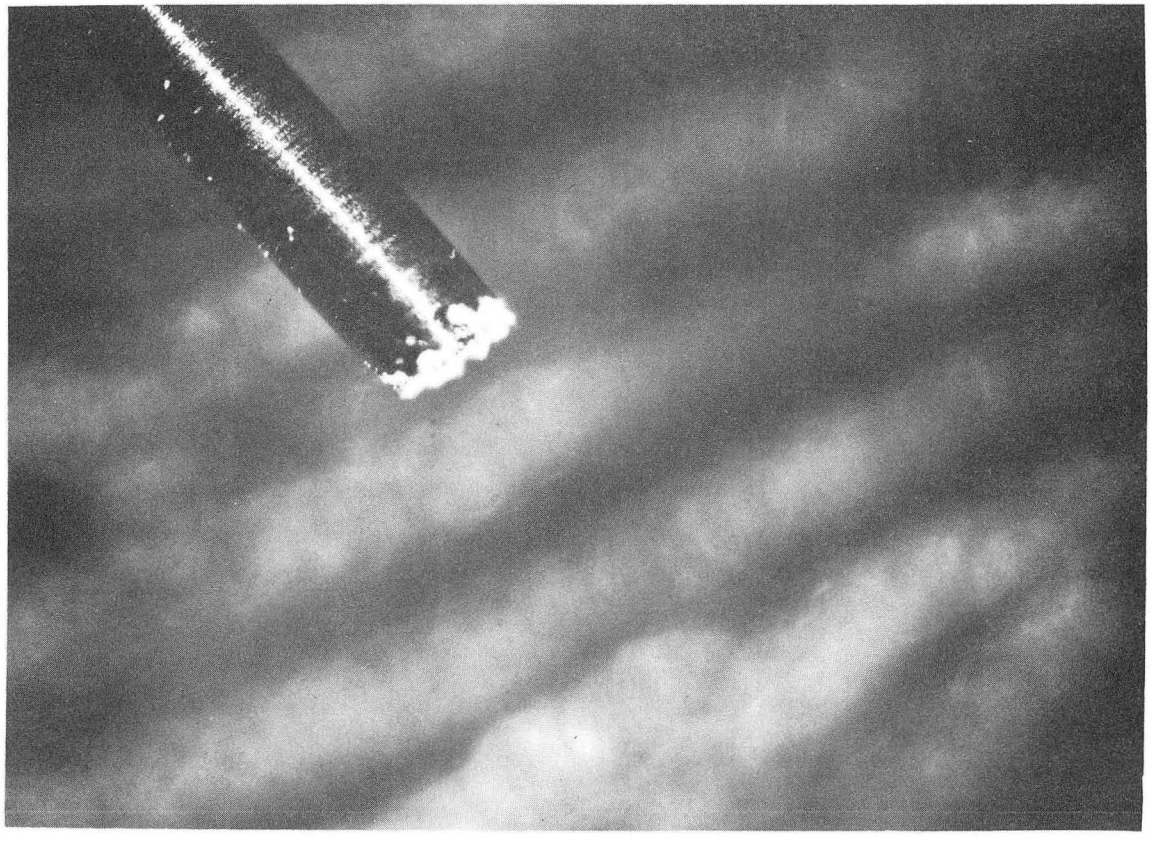

ZN-5242

Fig. 12

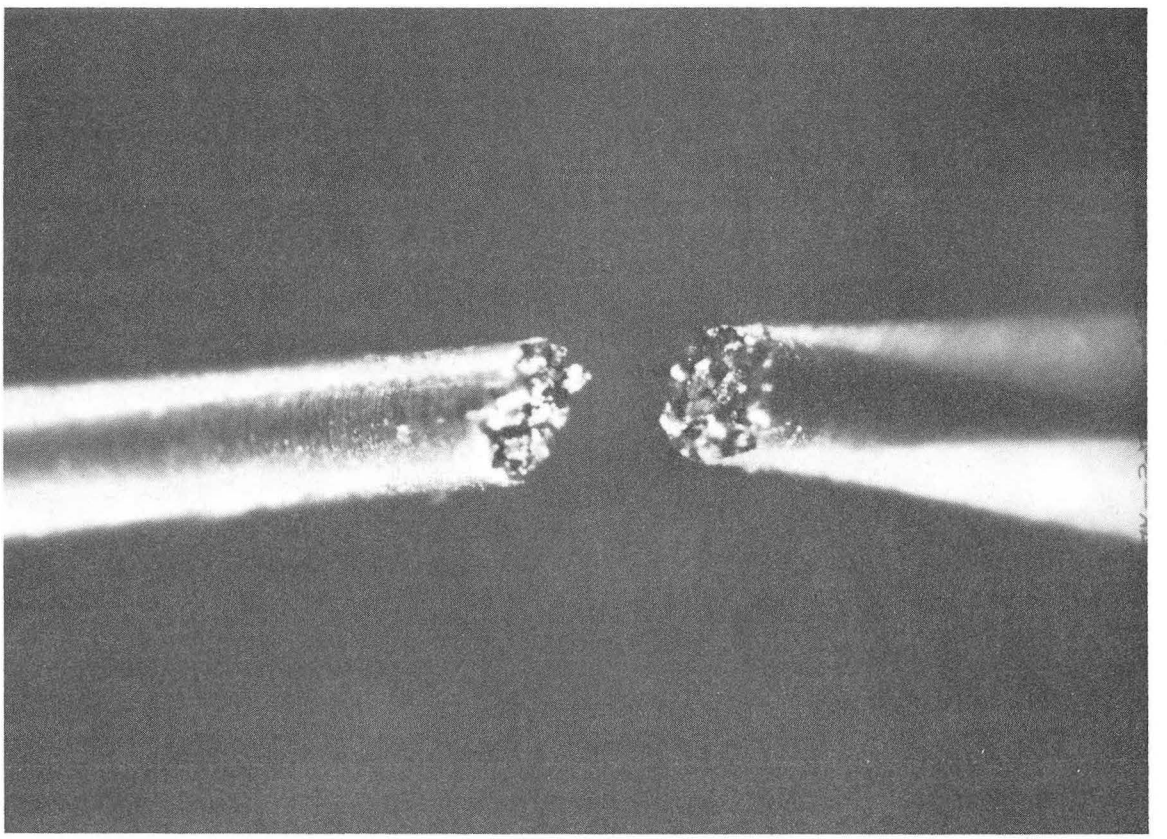

ZN-5792

Fig. 13

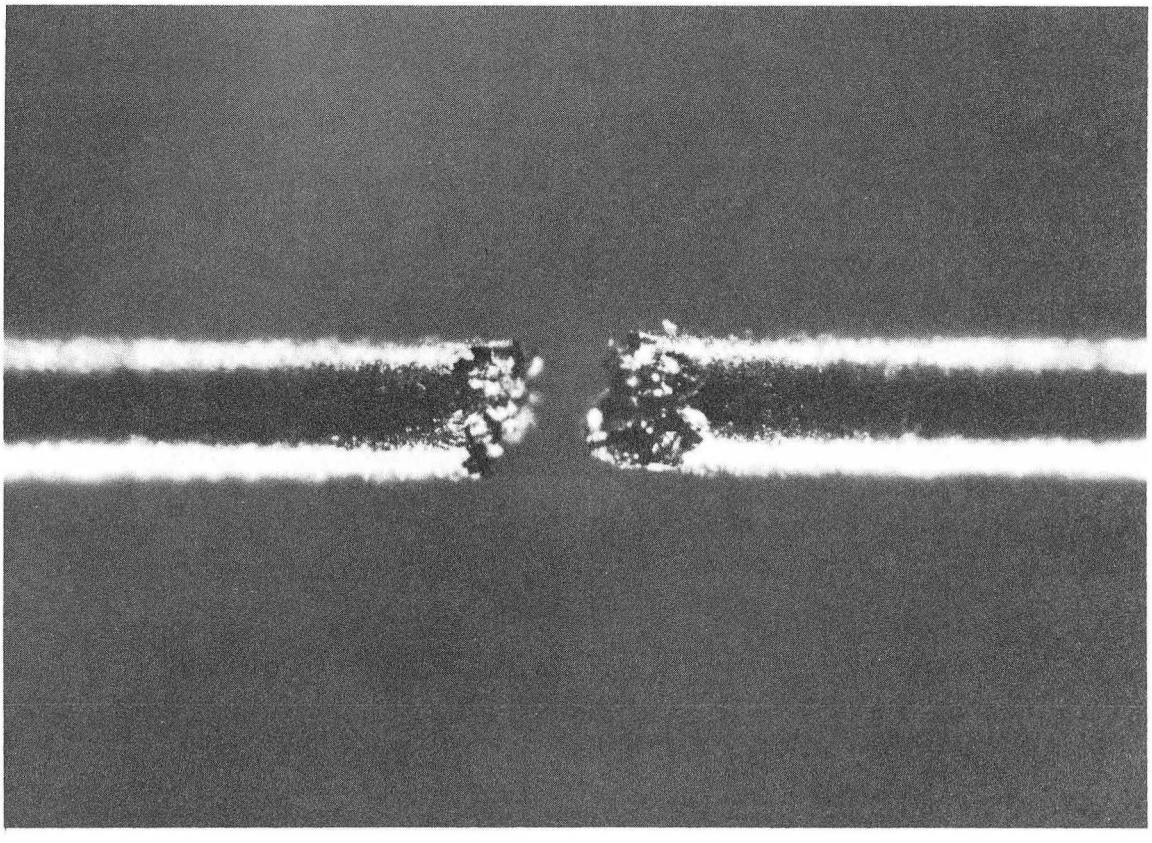

ZN-5793

Fig. 14

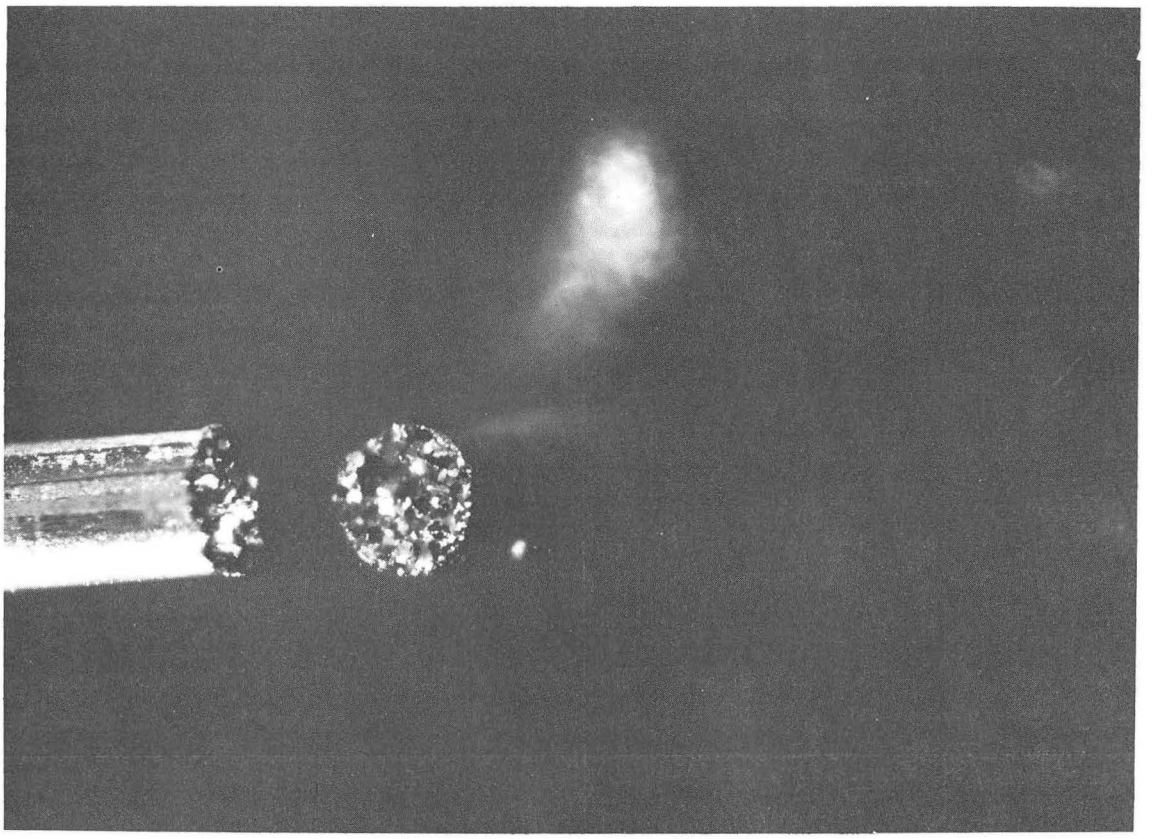

ZN-5238

Fig. 15

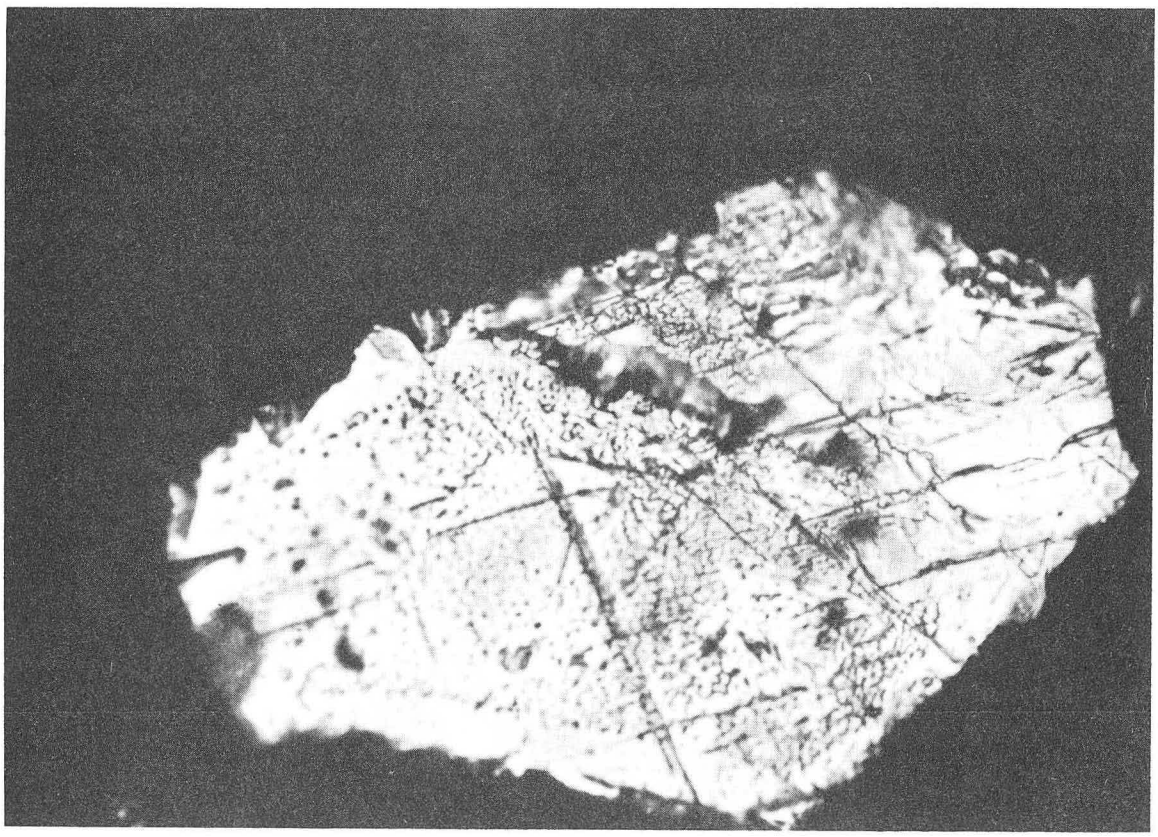

ZN-5794

Fig. 16

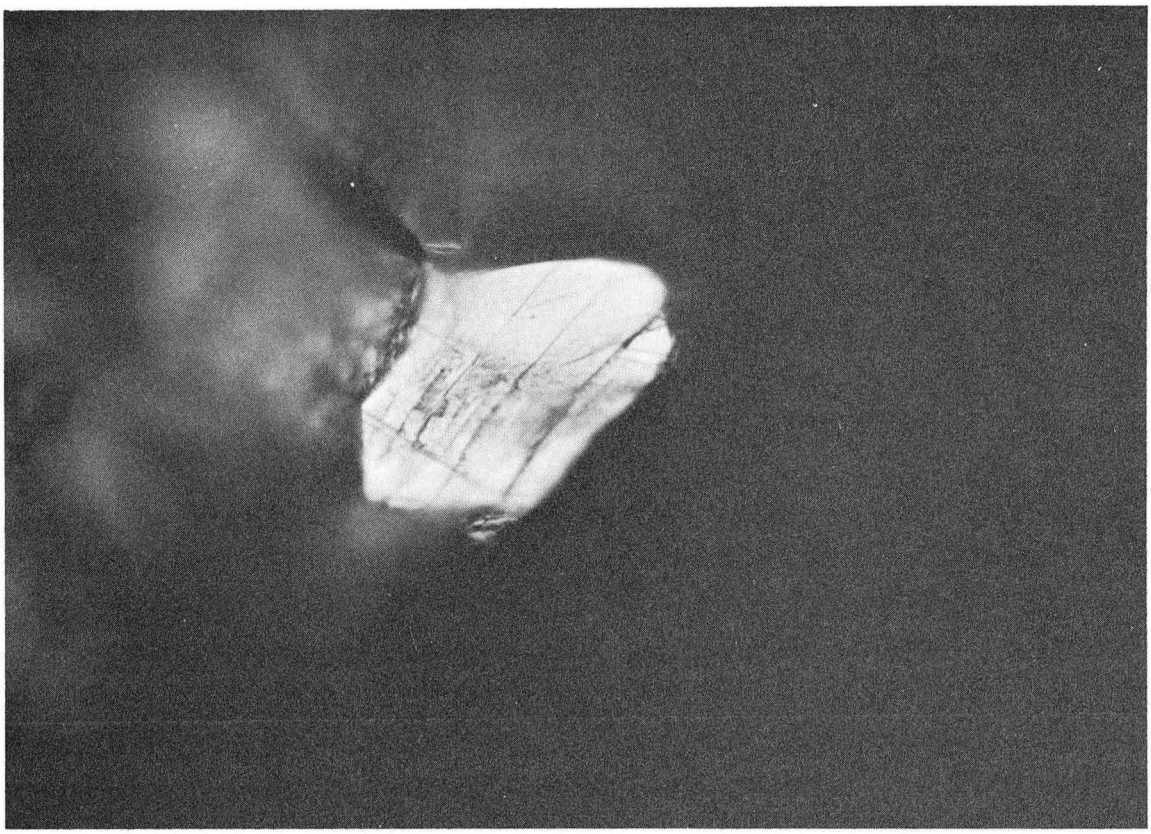

ZN-5795

Fig. 17

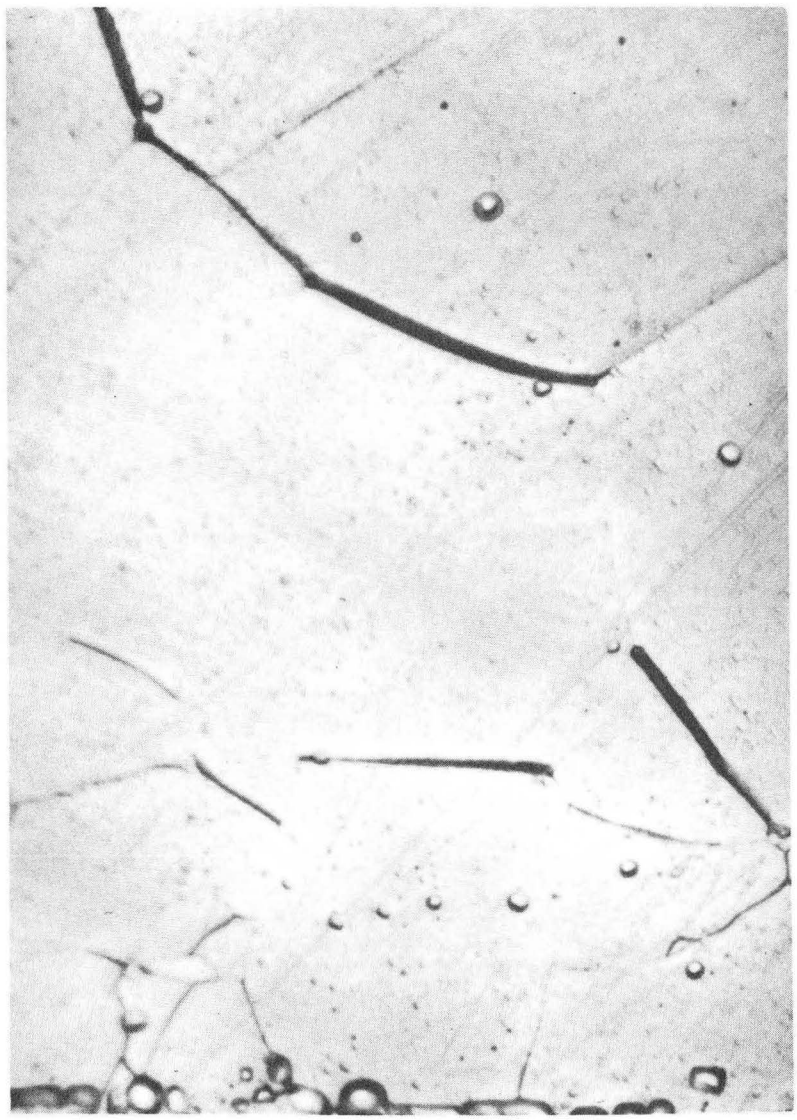

ZN-5748

Fig. 18

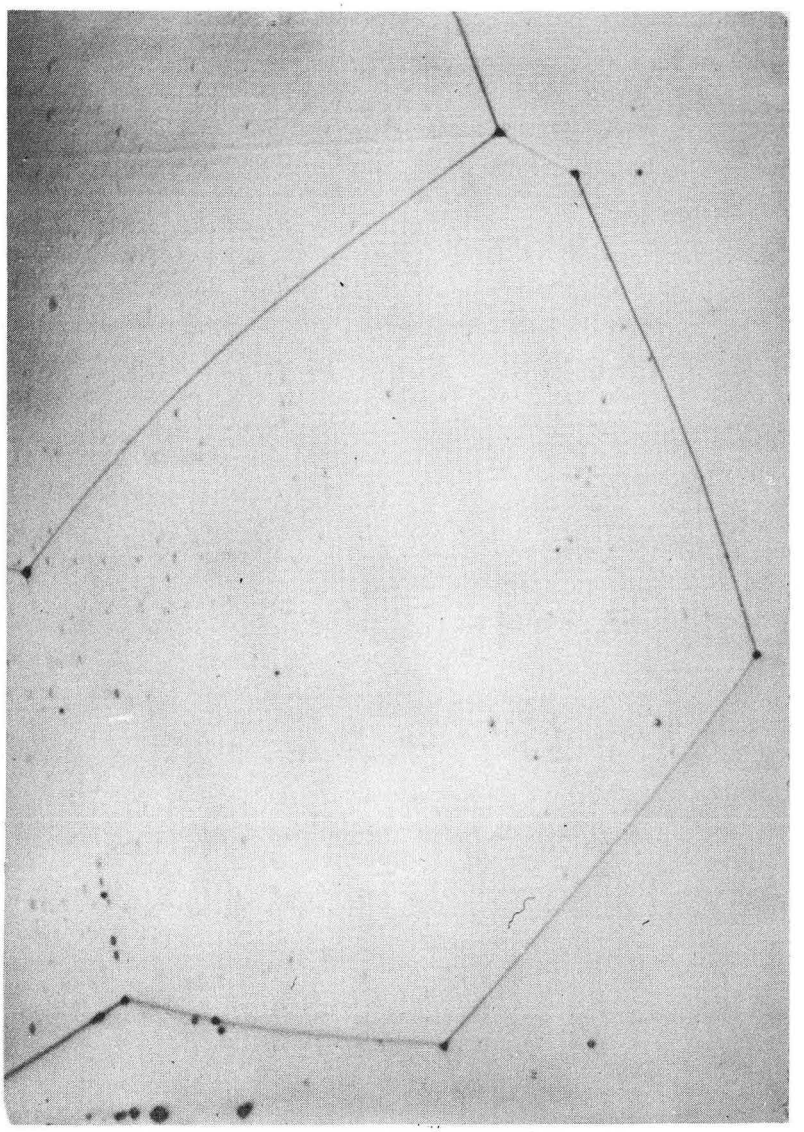

ZN-5749

Fig. 19a

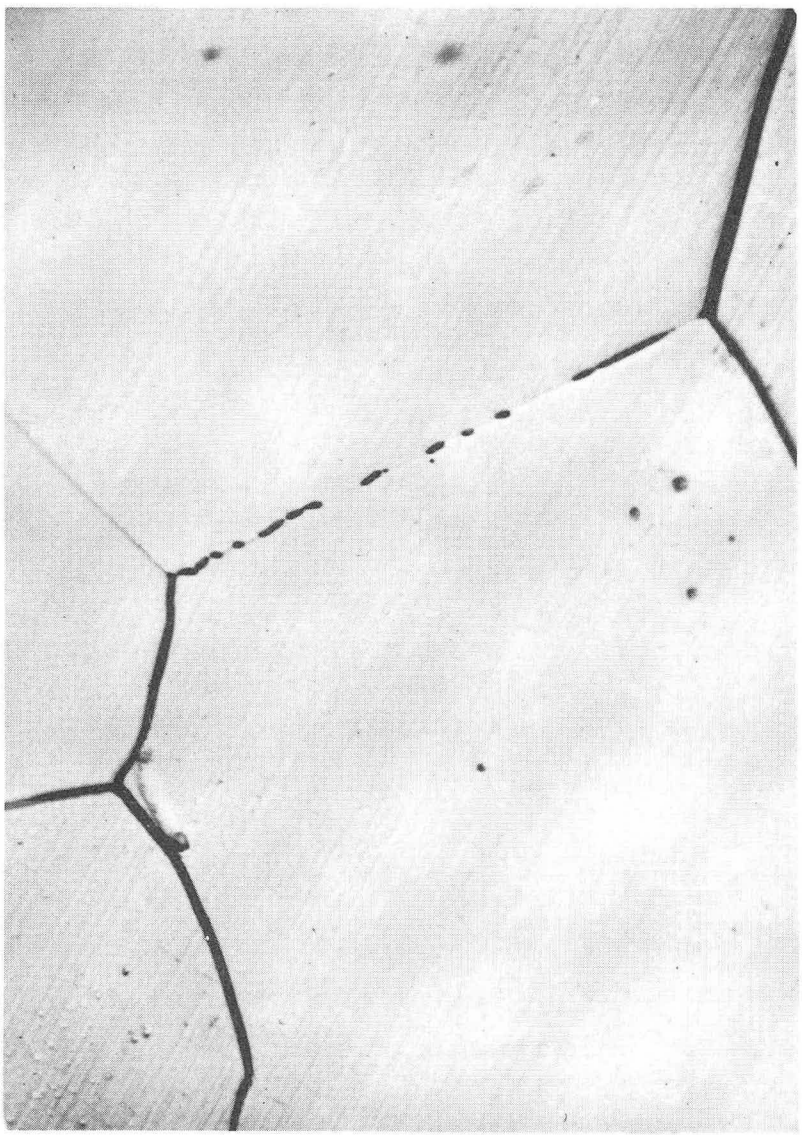

ZN-5750

Fig. 19b

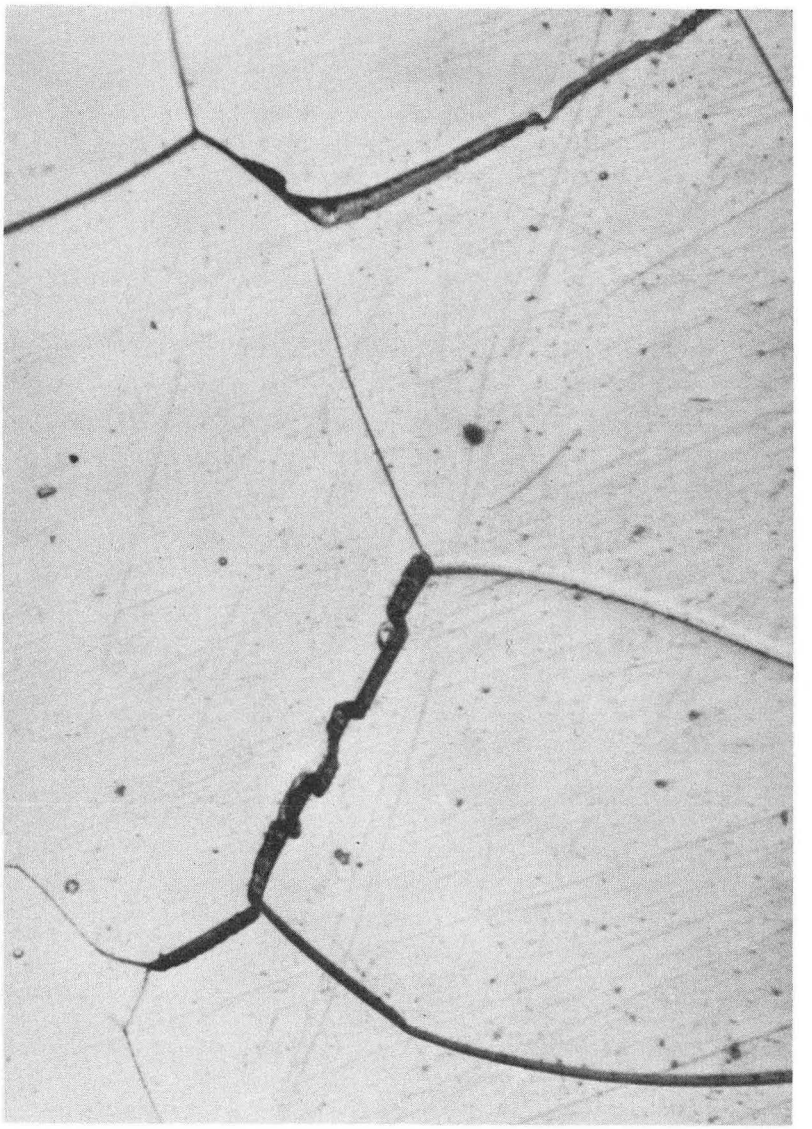

ZN - 5747

Fig. 20

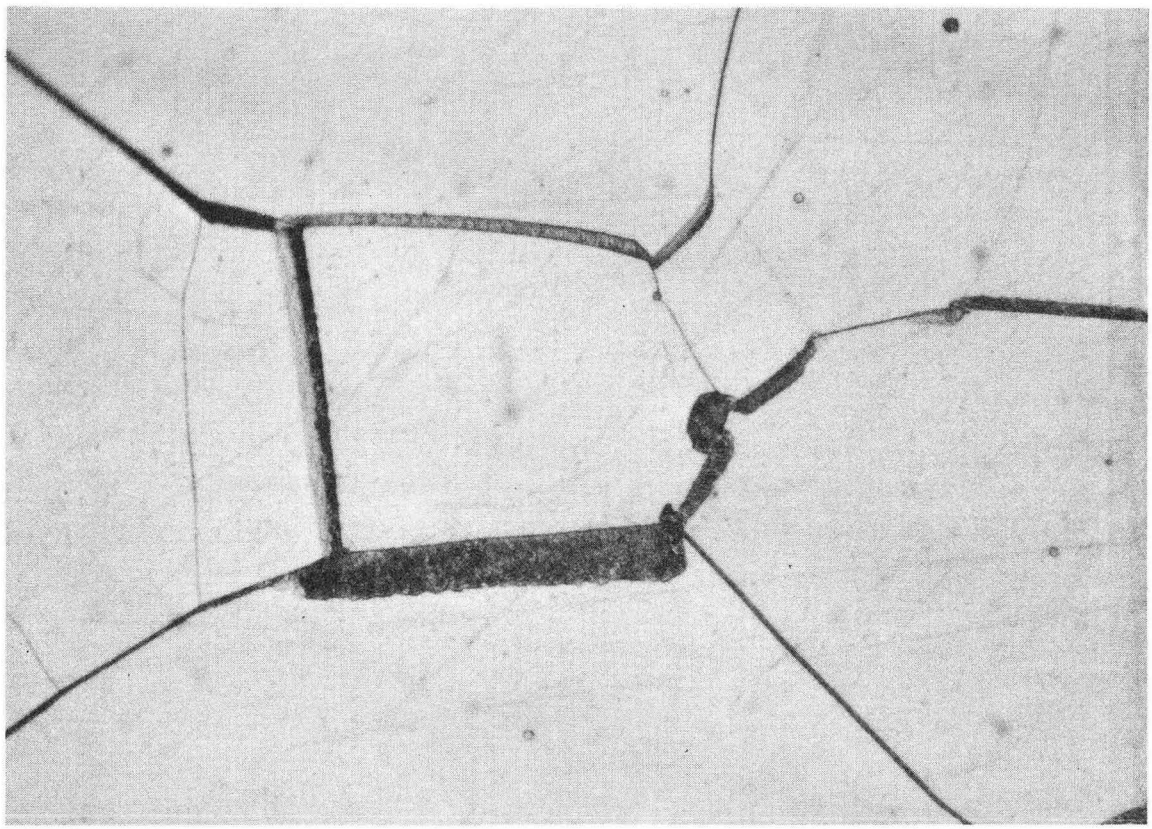

ZN-5796

Fig. 21

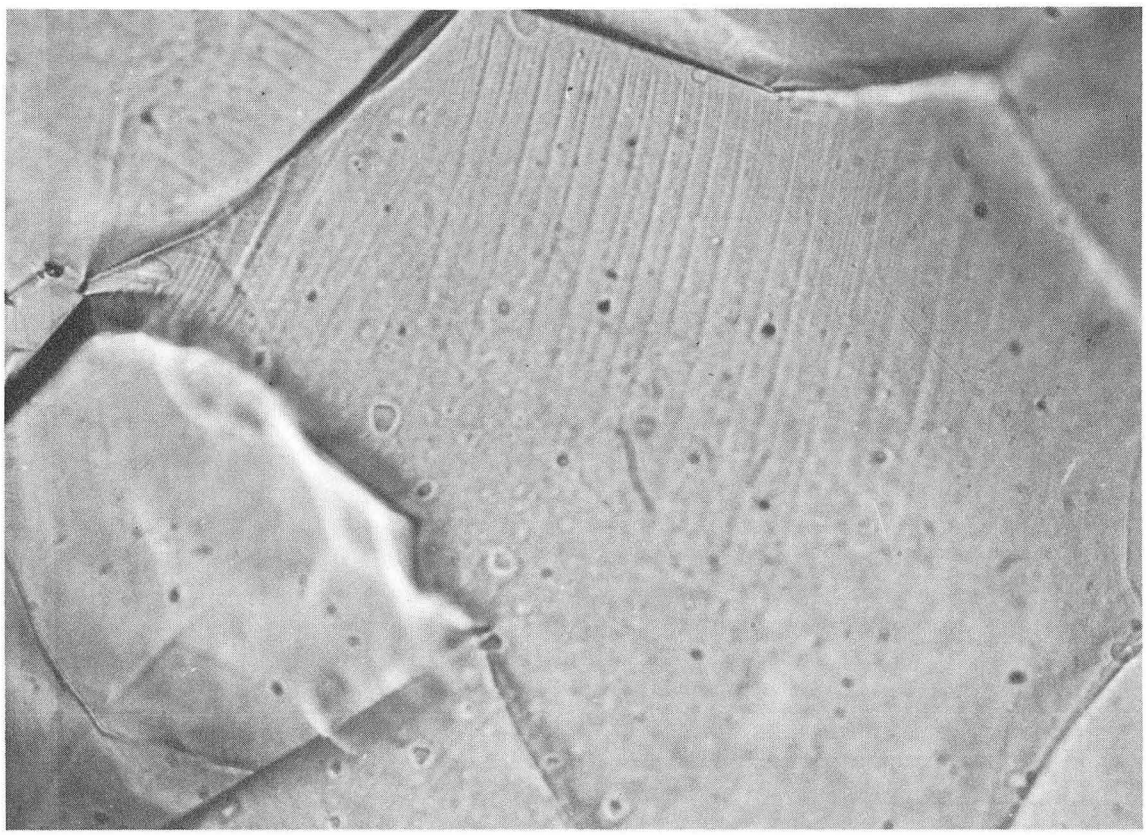

ZN-5797

Fig. 22

ZN-5798

Fig. 23

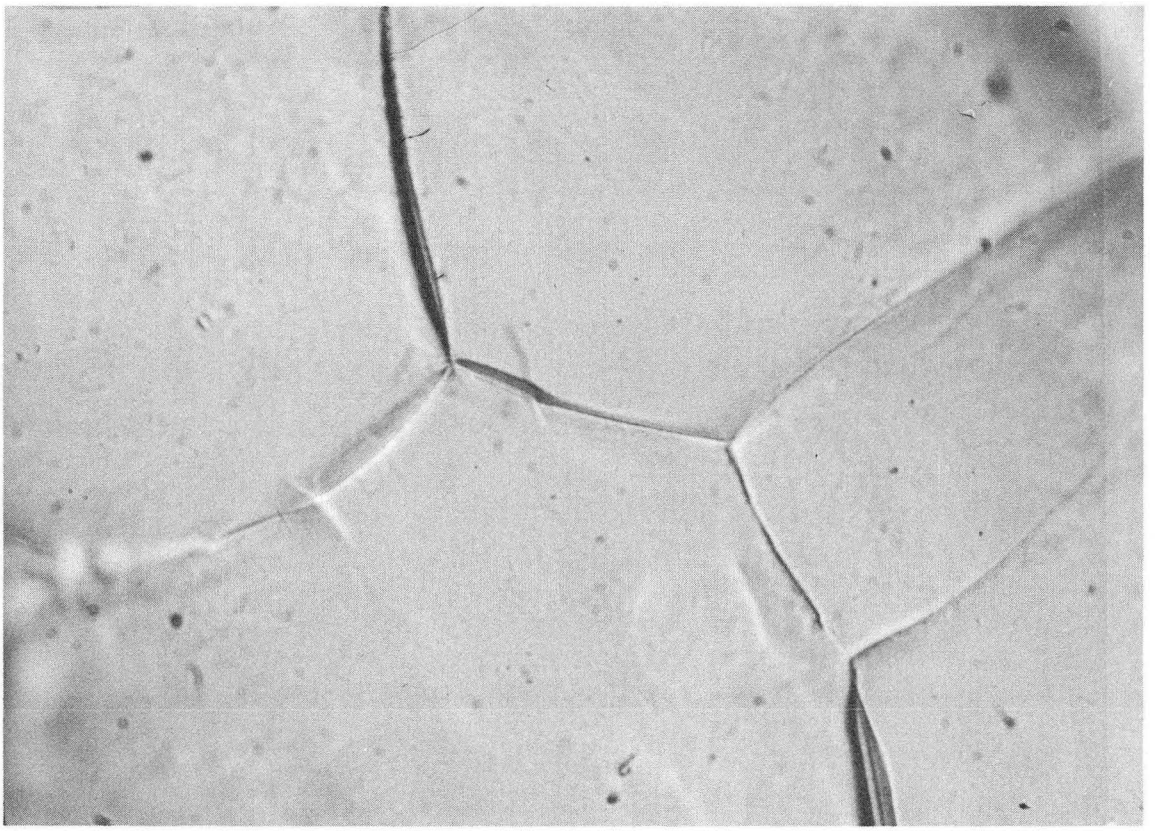

ZN-5799

Fig. 24

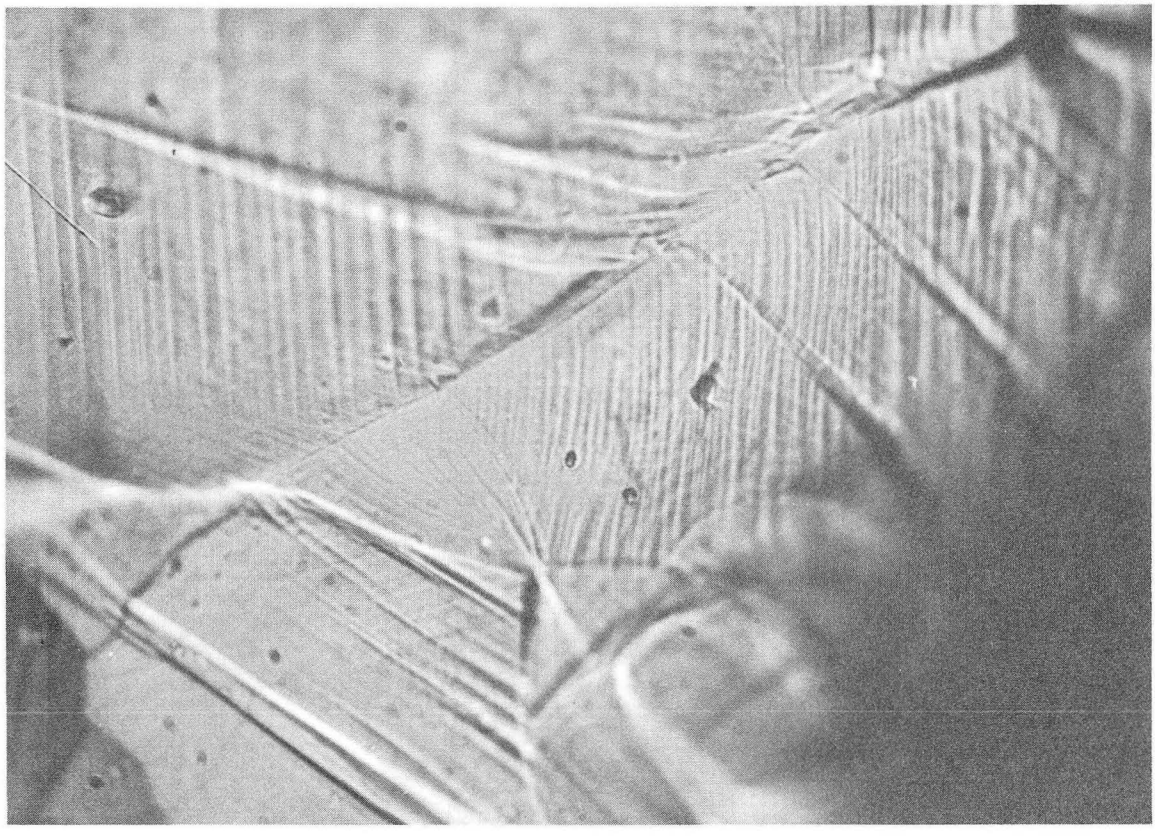

ZN-5800

Fig. 25

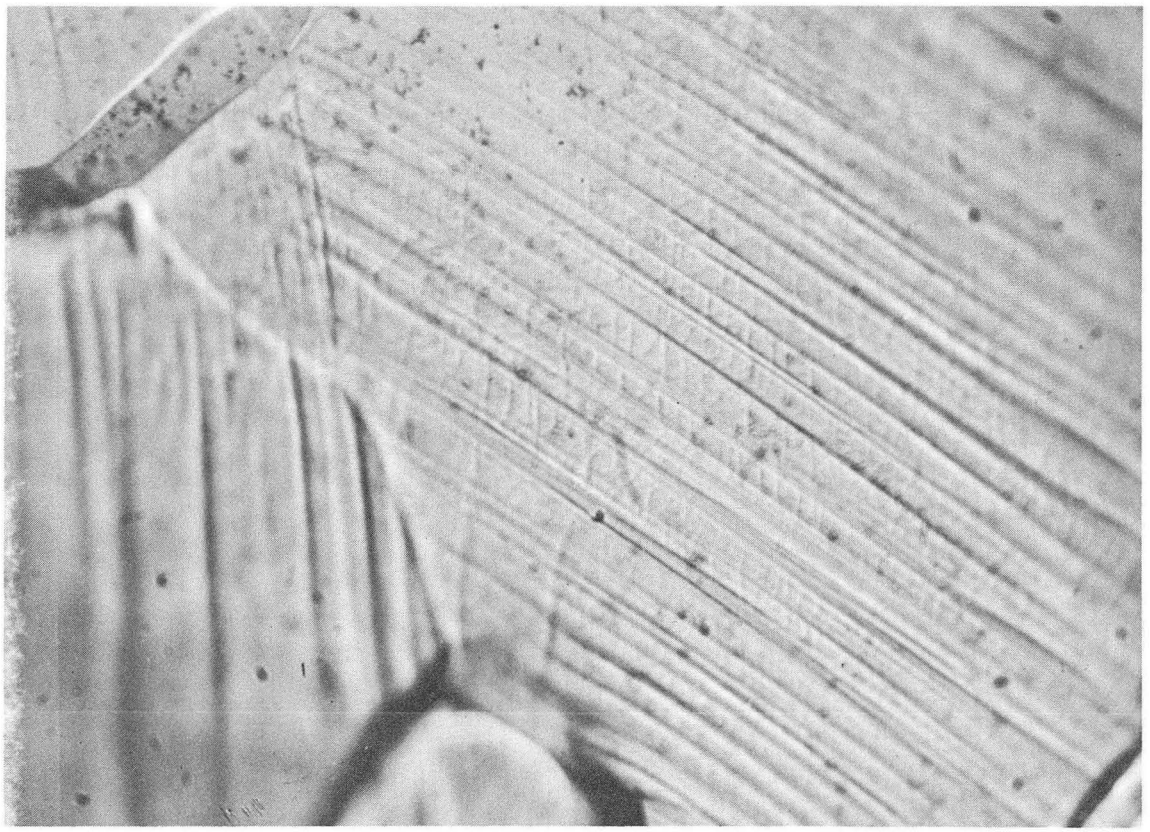

ZN-5801

Fig. 26

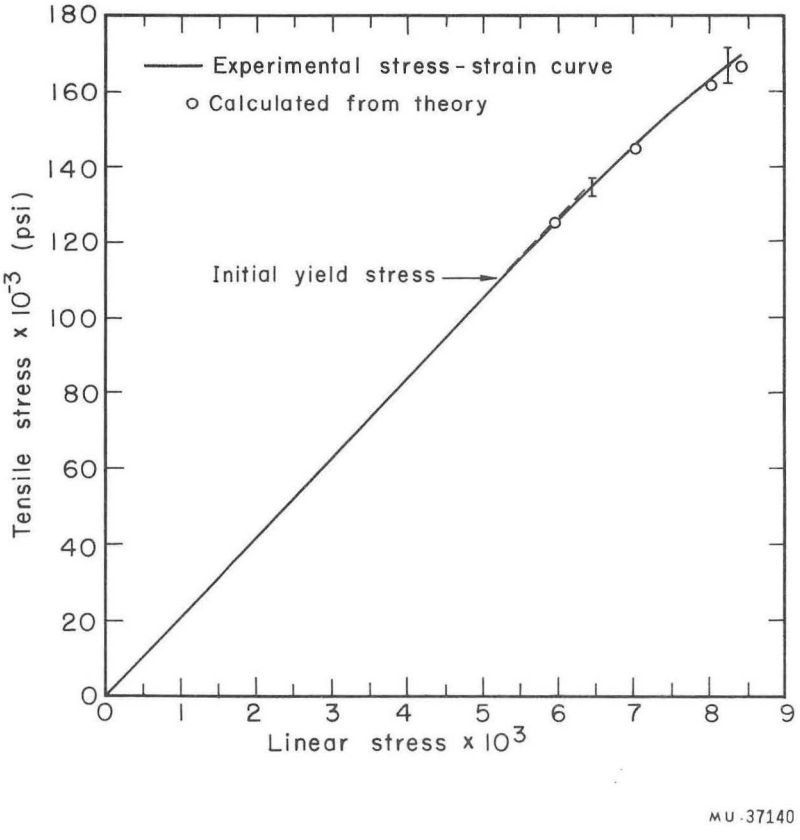
Experimental stress-strain curve
Calculated from theory
Initial yield stress
Tensile stress x 10^{-3} (psi)
Linear stress x 10^{3}
0
20
40
60
80
100
120
140
160
180
0
1
2
3
4
5
6
7
8
9
MU-37140

Fig. 27

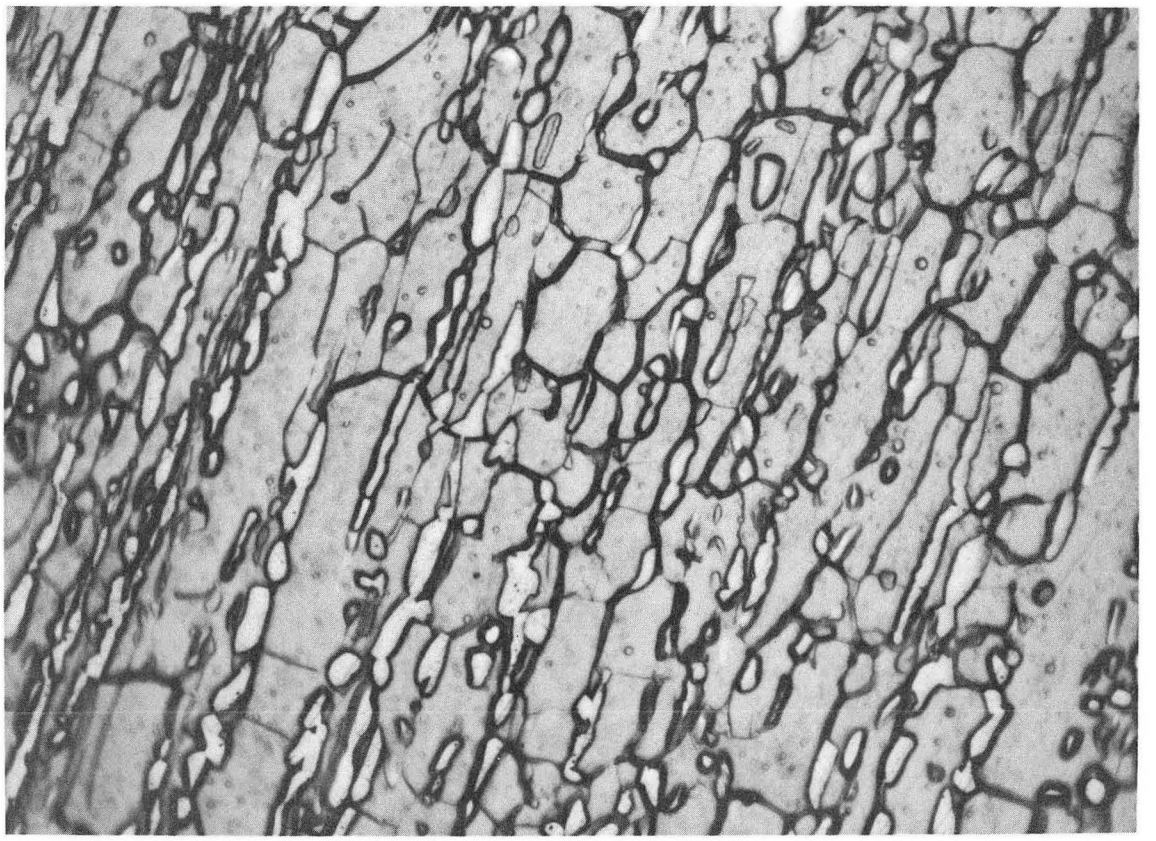

ZN-5236

Fig. 28

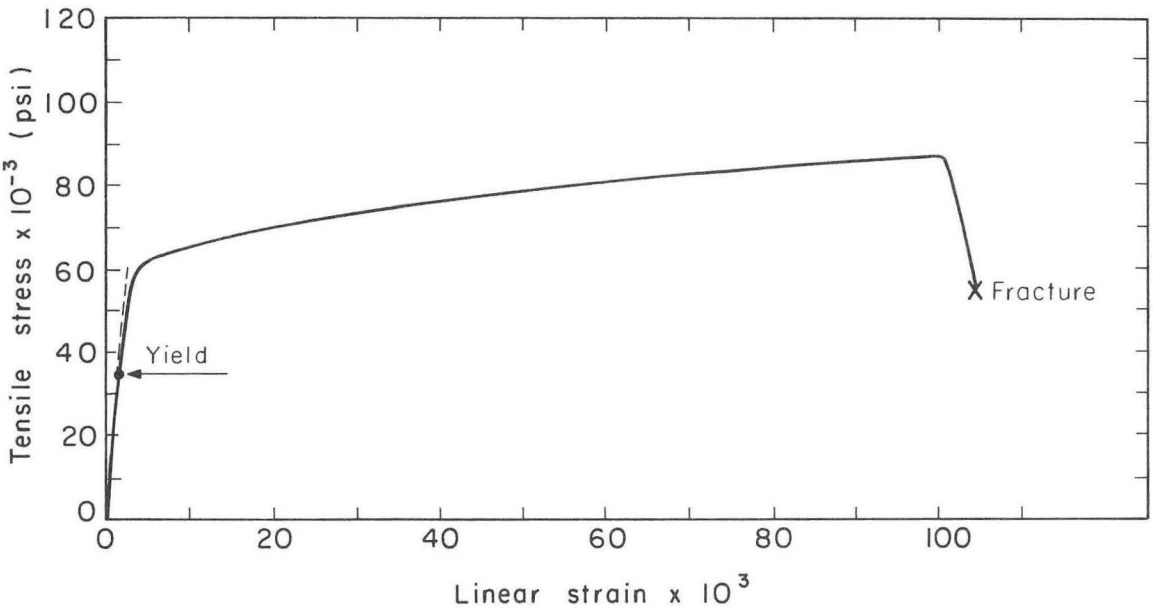
120
100
80
60
40
20
0
Tensile stress x 10^{-3} (psi)
0
20
40
60
80
100
Linear strain x 10^{3}
Yield
Fracture
MU-37189

Fig. 29

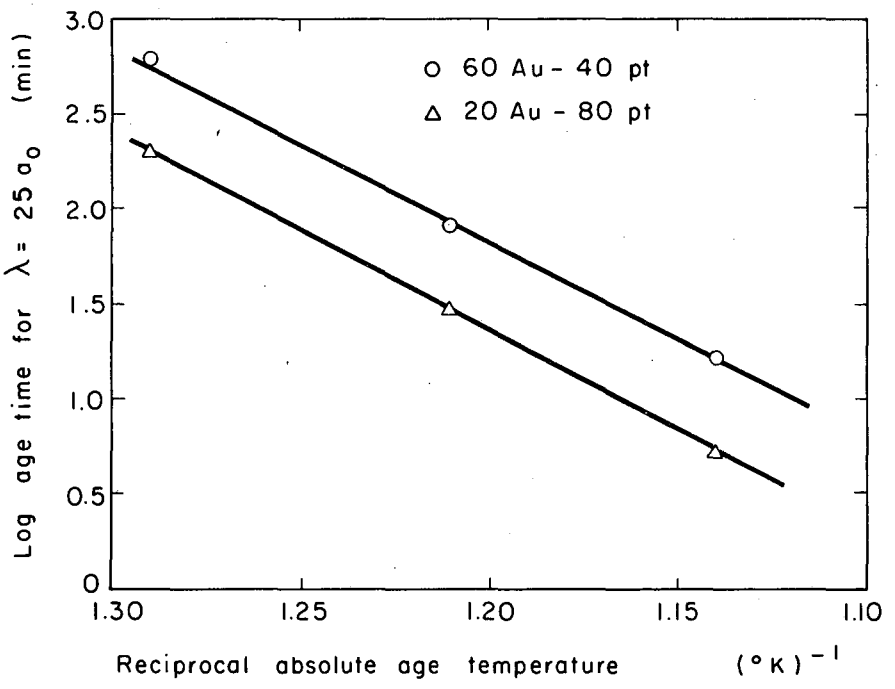
3.0
2.5
2.0
1.5
1.0
0.5
0
Log age time for λ = 25 a₀ (min)
o 60 Au - 40 pt
Δ 20 Au - 80 pt
1.30
1.25
1.20
1.15
1.10
Reciprocal absolute age temperature (°K)⁻¹
MU-37203

Fig. 30

APPENDIX A

Experimental Stress-Strain Curves for Tensile Tests

(All curves for 60% gold - 40% platinum alloys.)

Fig. A1 - Specimens in homogenized and quenched condition

Fig. A2 - Specimen aged 1/2 hour at 510°C.

Fig. A3 - Specimen aged 1 hour at 510°C.

Fig. A4 - Specimen aged 5 hours at 510°C.

Fig. A5 - Specimens aged 10 hours at 510°C.

Fig. A6 - Specimens aged 20 hours at 510°C.

Fig. A7 - Specimens aged 98 hours at 510°C.

Fig. A8 - Specimen aged 5 hours at 410°C.

Fig. A9 - Specimen aged 10 hours at 410°C.

Fig. A10- Specimen aged 40 hours at 410°C.

Fig. A11- Specimens aged 200 hours at 410°C.

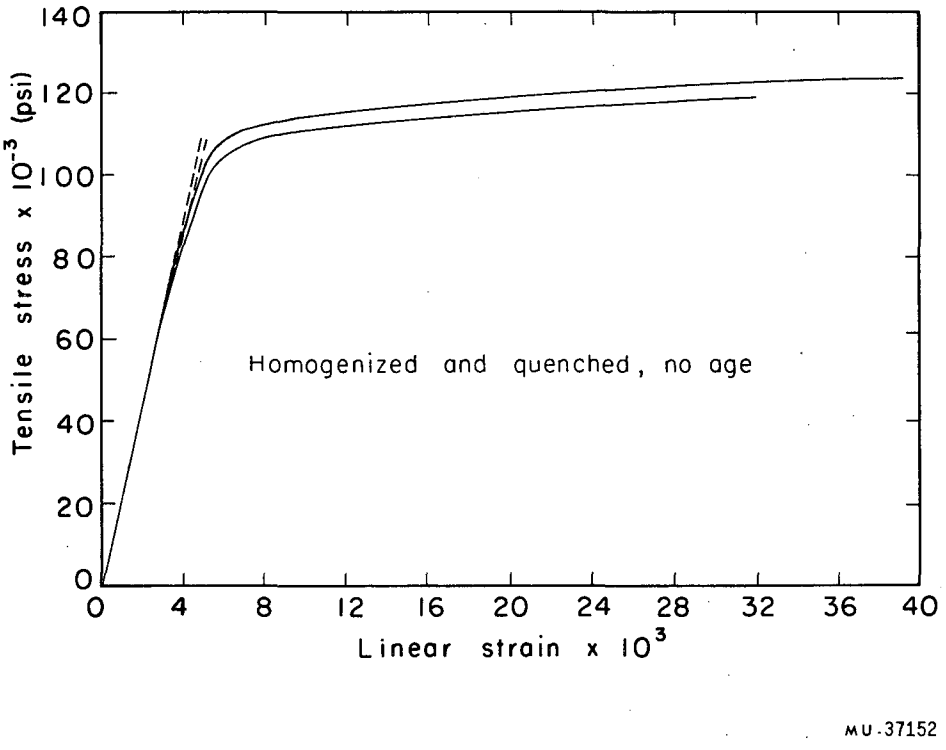
Tensile stress x 10^{-3} (psi)
140
120
100
80
60
40
20
0
0
4
8
12
16
20
24
28
32
36
40
Linear strain x 10^{3}
Homogenized and quenched, no age
MU-37152

Fig. A1

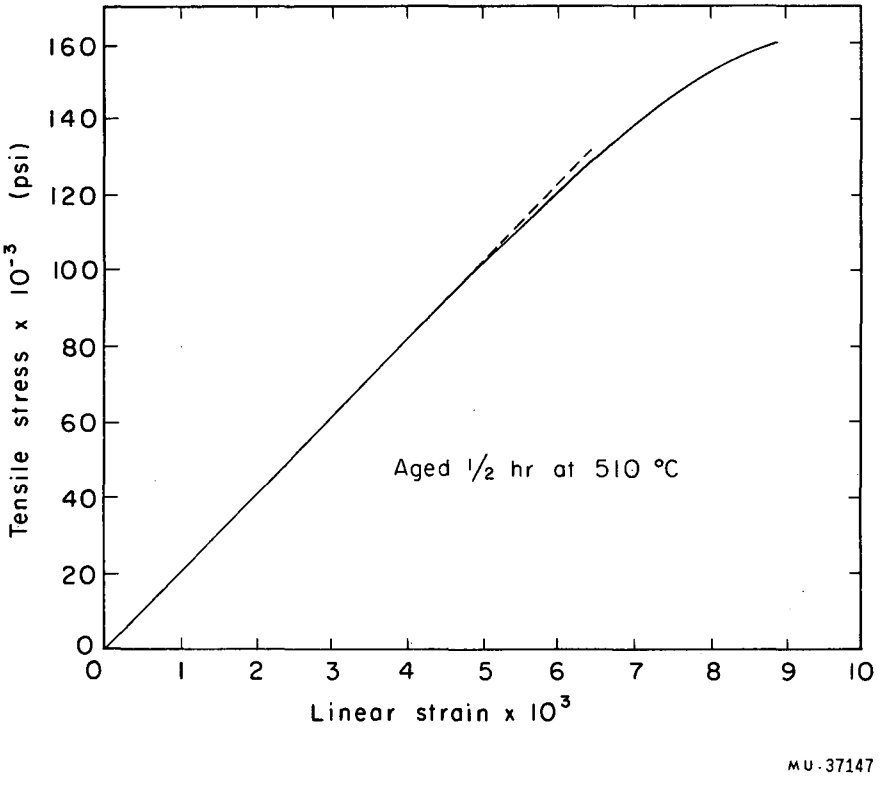
Tensile stress x 10^{-3} (psi)
160
140
120
100
80
60
40
20
0
0
1
2
3
4
5
6
7
8
9
10
Linear strain x 10^{3}
Aged 1/2 hr at 510 °C
MU-37147

Fig. A2

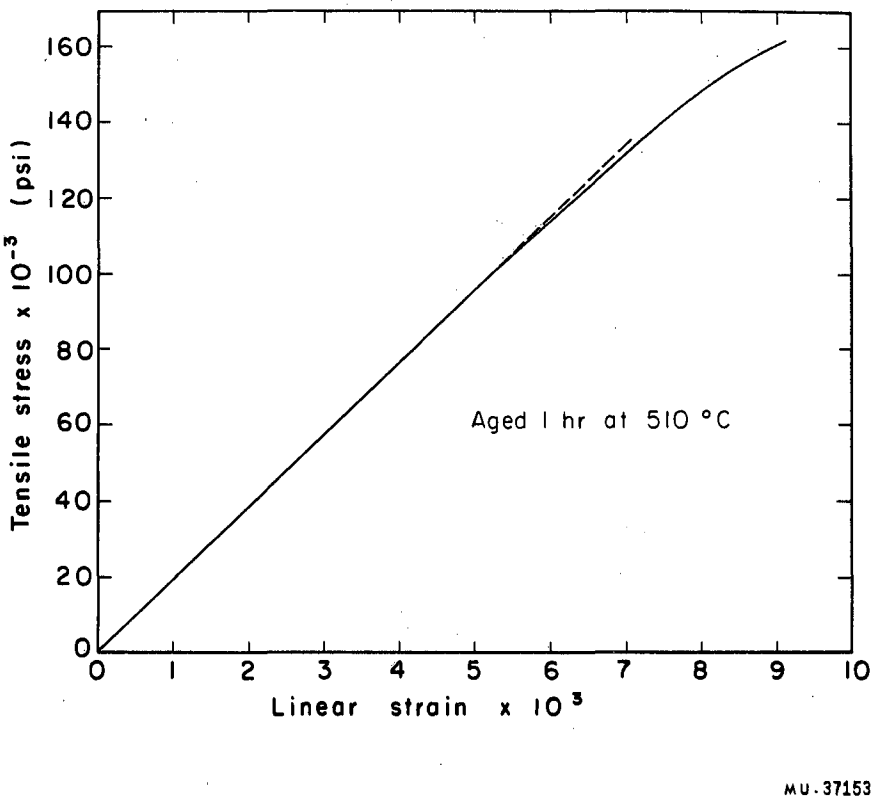
Tensile stress x 10^{-3} (psi)
160
140
120
100
80
60
40
20
0
0
1
2
3
4
5
6
7
8
9
10
Linear strain x 10^{3}
Aged 1 hr at 510 °C
MU-37153

Fig. A3

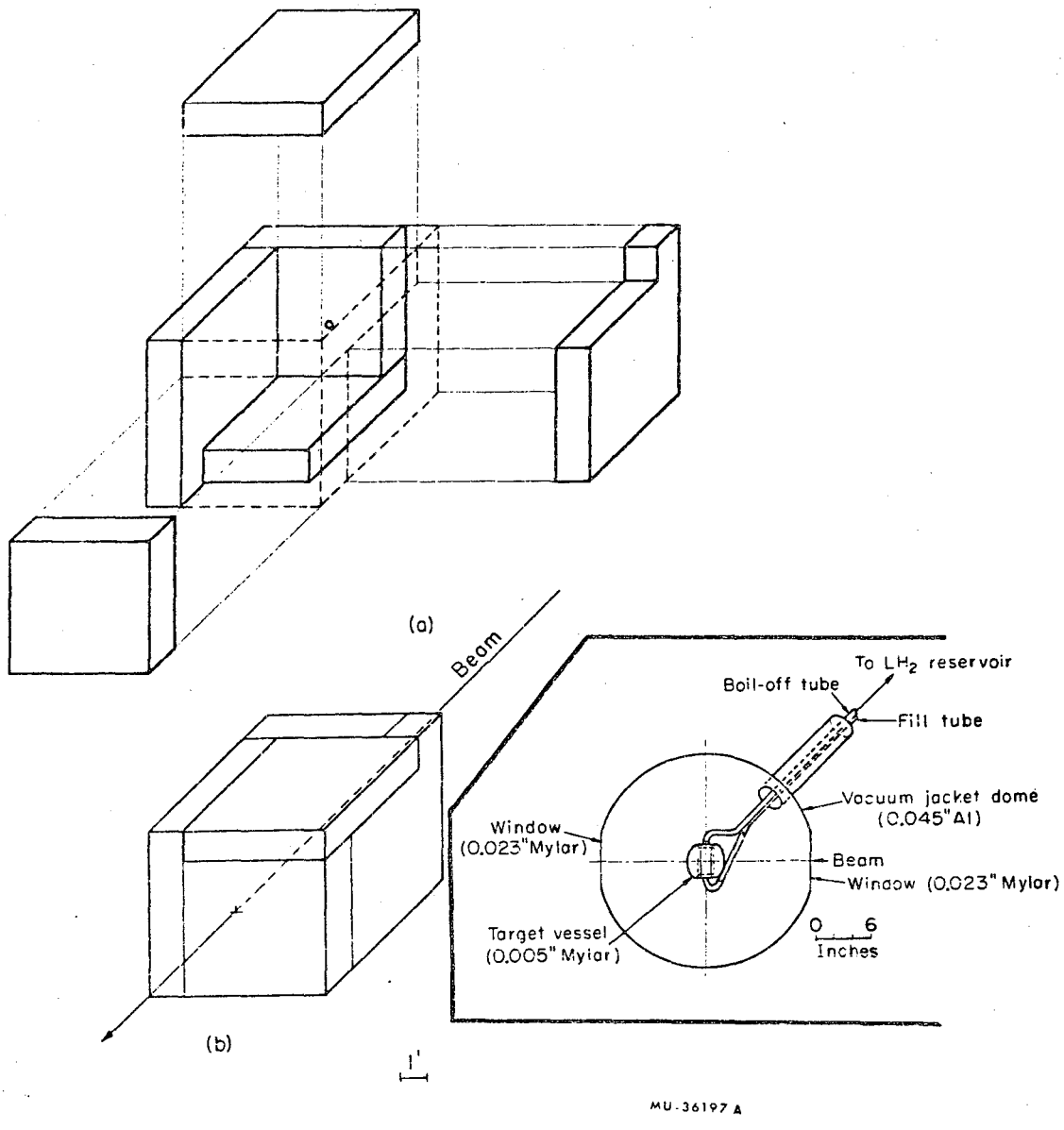
(a)
Beam
(b)
1'
To LH_2 reservoir
Boil-off tube
Fill tube
Vacuum jacket dome
(0.045" Al)
Window
(0.023" Mylar)
Beam
Window (0.023" Mylar)
Target vessel
(0.005" Mylar)
0 6
Inches
MU-36197 A

Fig. 3

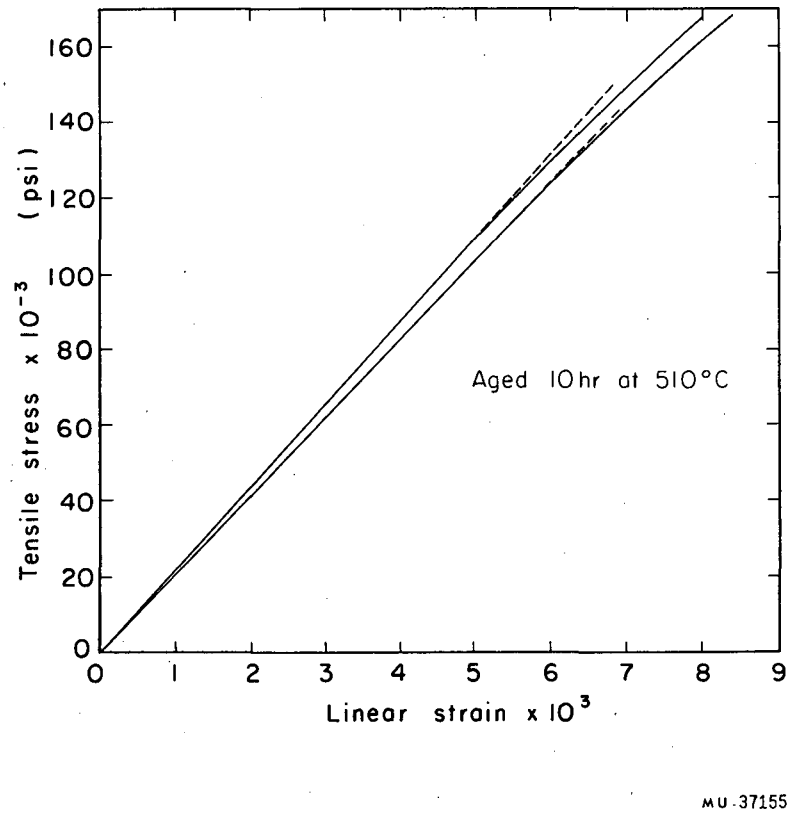
Tensile stress x 10^{-3} (psi)
160
140
120
100
80
60
40
20
0
0
1
2
3
4
5
6
7
8
9
Linear strain x 10^{3}
Aged 10 hr at 510°C
MU-37155

Fig. A5

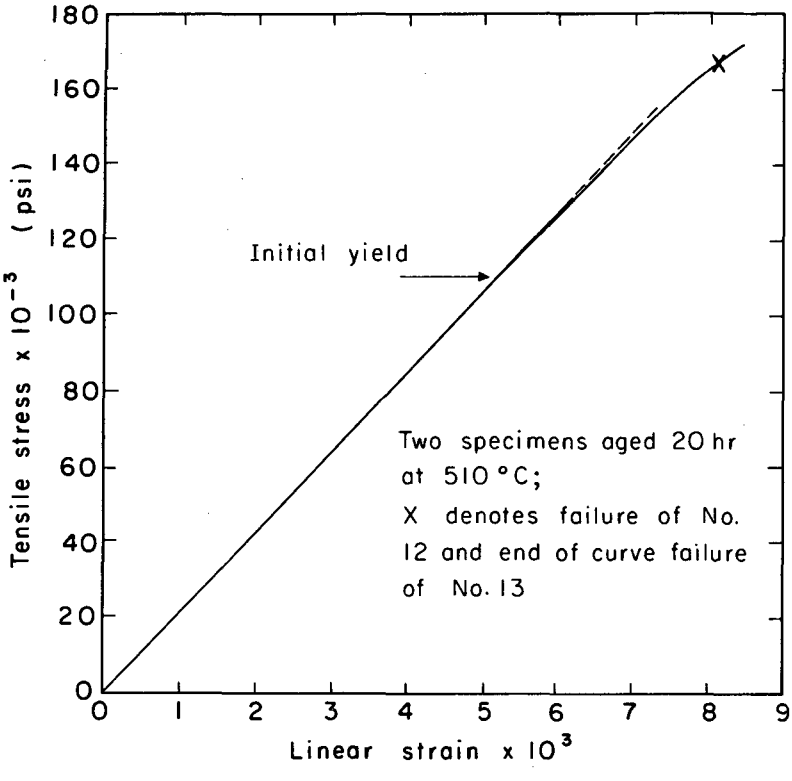
180
160
140
120
100
80
60
40
20
0
Tensile stress x 10^{-3} (psi)
0
1
2
3
4
5
6
7
8
9
Linear strain x 10^{3}
Initial yield
Two specimens aged 20 hr at 510 °C;
X denotes failure of No. 12 and end of curve failure of No. 13
MU-37148

Fig. A6

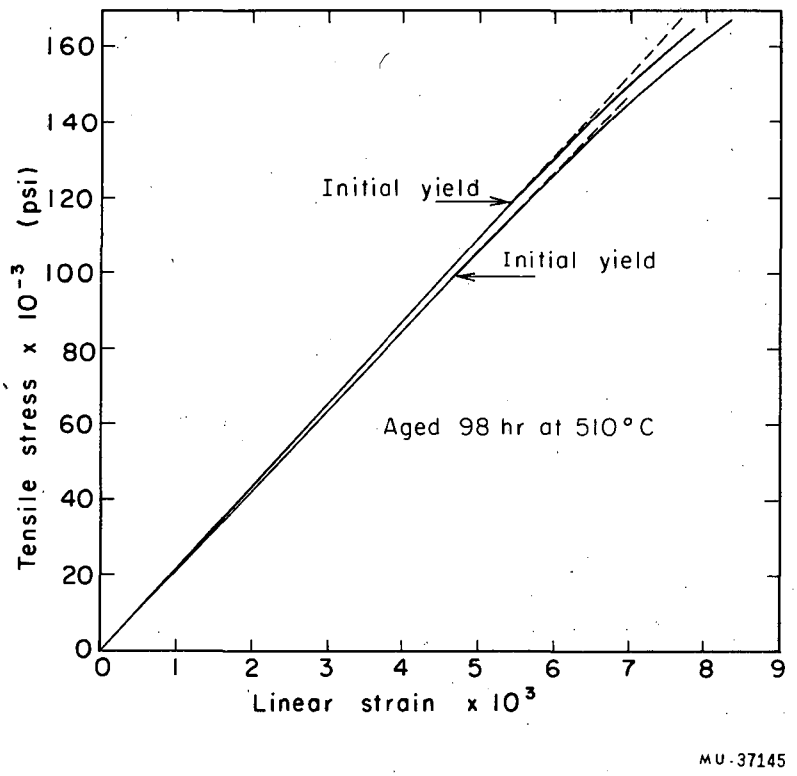
160
140
120
100
80
60
40
20
0
Tensile stress x 10^{-3} (psi)
Initial yield
Initial yield
Aged 98 hr at 510°C
0
1
2
3
4
5
6
7
8
9
Linear strain x 10^{3}
MU-37145

Fig. A7

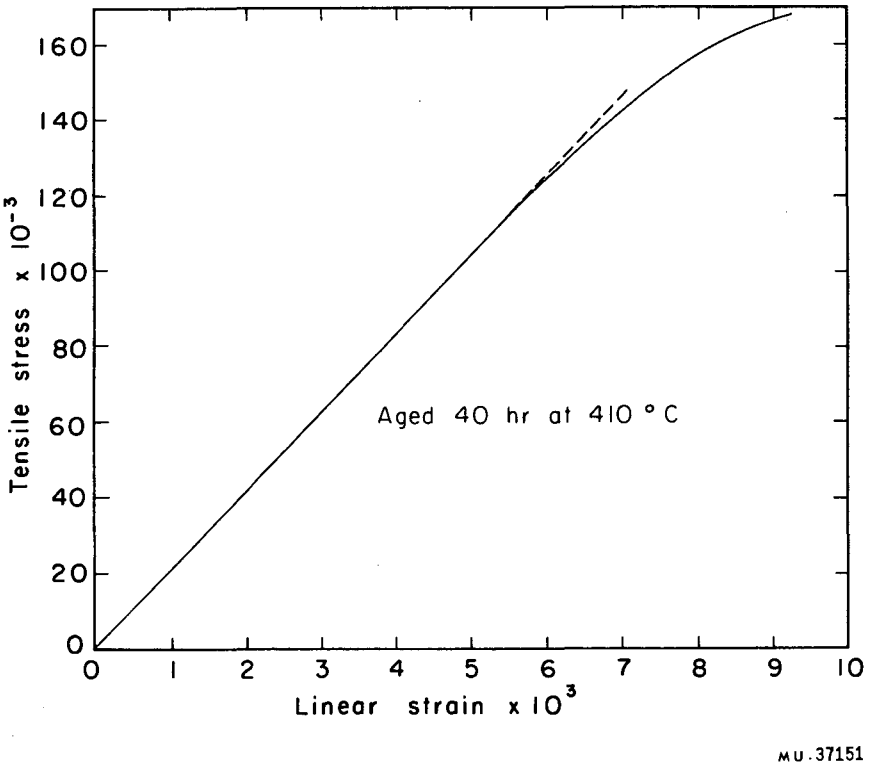
Tensile stress x 10^{-3}
Linear strain x 10^{3}
Aged 40 hr at 410 °C
0
20
40
60
80
100
120
140
160
0
1
2
3
4
5
6
7
8
9
10
MU.37151

Fig. A10

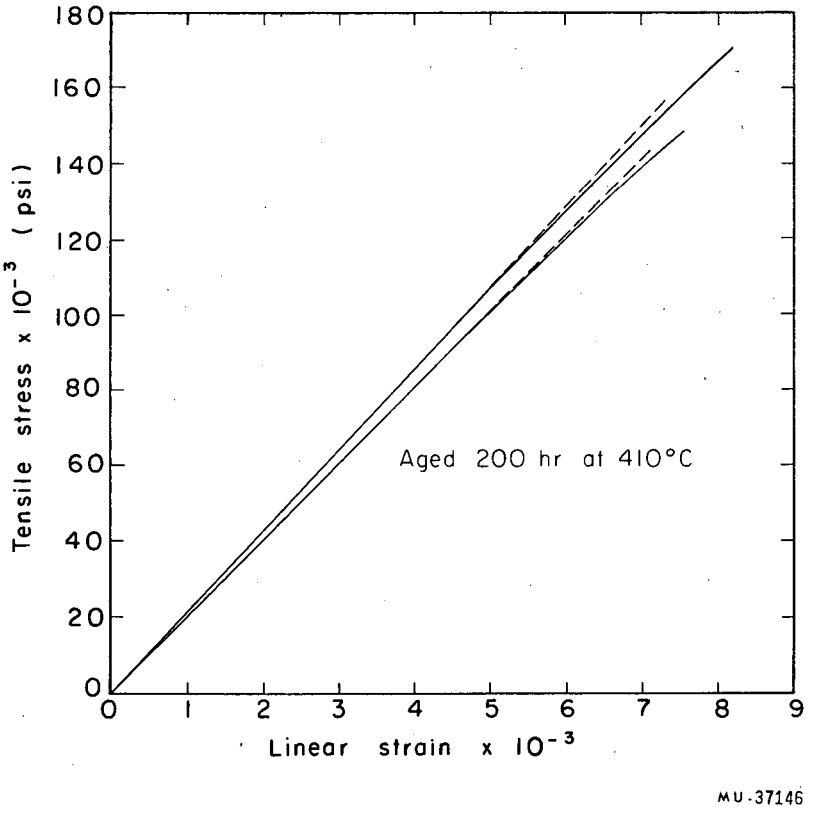
180
160
140
120
100
80
60
40
20
0
Tensile stress x 10^{-3} (psi)
0
1
2
3
4
5
6
7
8
9
Linear strain x 10^{-3}
Aged 200 hr at 410°C
MU-37146

Fig. A11

APPENDIX B*

Debye-Scherrer X-Ray Patterns for Alloy Specimens

Fig. B-1 20% gold - 80% platinum alloy aged at 550°C.

(1) aged 10 minutes

(2) aged 30 minutes

(3) aged 1 hour

(4) aged 3 hours

(5) aged 5 hours

(6) aged 7 hours

Fig. B-2 60% gold - 40% platinum alloy aged at 550°C.

(1) aged 10 minutes

(2) aged 30 minutes

(3) aged 1 hour

(4) aged 3 hours

(5) aged 5 hours

(6) aged 7 hours

Fig. B-3 20% gold - 80% platinum alloy aged at 500°C.

(1) homogenized and quenched, no age

(2) aged 30 minutes

(3) aged 2 hours

(4) aged 5 hours

(5) aged 10 hours

(6) aged 20 hours

Fig. B-4 60% gold - 40% platinum alloy aged at 500°C.

(1) aged 30 minutes

(2) aged 2 hours

(3) aged 5 hours

(4) aged 10 hours

(5) aged 15 hours

(6) aged 20 hours

Fig. B-5 60% gold - 40% platinum alloy aged at 410°C.

(1) aged 5 hours

(2) aged 10 hours

(3) aged 40 hours

(4) aged 200 hours

*Appendix B figures have been omitted from this report because of reproduction difficulties. A copy is on file with the Engineering Department, University of California, Berkeley.